Surfactant induced gelation of TEMPO-oxidized cellulose nanofibril dispersions probed using small angle neutron scattering

Julien Schmitt, Vincenzo Calabrese, Marcelo A da Silva, Kazi M Z Hossain, Peixun Li, Najet Mahmoudi, Robert M Dalgliesh, Adam L Washington, Janet L Scott, Karen J Edler

Surfactant induced gelation of TEMPO-oxidised cellulose nanofibril dispersions probed using small angle neutron scattering

Cite as: J. Chem. Phys. (in press) (2022); https://doi.org/10.1063/5.0129276
Submitted: 04 October 2022 • Accepted: 20 December 2022 • Accepted Manuscript Online: 20 December 2022

Julien Schmitt, **Vincenzo Calabrese,** **Marcelo A da Silva, et al.**

Accepted to J. Chem. Phys. 10.1063/5.0129276

Surfactant induced gelation of TEMPO-oxidised cellulose nanofibril dispersions probed using small angle neutron scattering

Julien Schmitt,[1,2] Vincenzo Calabrese,[1,3] Marcelo A. da Silva,[1,4] Kazi M. Z. Hossain,[1] Peixun Li,[5] Najet Mahmoudi,[5] Robert M. Dalgliesh,[5] Adam L. Washington,[5] Janet L. Scott[1,6] and Karen J. Edler[1,7*]

[1]Department of Chemistry, University of Bath, Bath BA2 7AY, UK
[2]current address: LSFC – Laboratoire de Synthèse et Fonctionnalisation des Céramiques, UMR 3080 CNRS/Saint-Gobain CREE, Saint-Gobain Research Provence, 550 Avenue Alphonse Jauffret, Cavaillon, France
[3] current address: Okinawa Institute of Science and Technology Graduate University, 1919-1 Tancha, Onna-son, Okinawa 904-0495, Japan
[4]current address: School of Life and Medical Sciences, University of Hertfordshire, Hatfield, Hertfordshire AL10 9AB, UK
[5]ISIS Neutron and Muon Source, Science and Technology Facilities Council, Rutherford Appleton Laboratory, Didcot OX11 0QX, UK
[6]Centre for Sustainable Chemical Technologies, University of Bath, Claverton Down, Bath, BA2 7AY, United Kingdom.
[7]current address: Center for Analysis and Synthesis, Department of Chemistry, Lund University, SE-22100 Lund, Sweden

* Corresponding author email karen.edler@chem.lu.se

Abstract

In this work, we studied TEMPO-oxidised cellulose nanofibrils (OCNF) suspensions in presence of diverse surfactants. Using a combination of small angle neutron scattering (SANS) and rheology, we compared the physical properties of the suspensions with their structural behaviour. Four surfactants were studied, all with the same hydrophobic tail length but different headgroups: hexaethylene glycol mono-n-dodecyl ether ($C_{12}EO_6$, non-ionic), sodium dodecyl sulphate (SDS, anionic), cocamidopropyl betaine (CapB, zwitterionic) and dodecyltrimethylammonium bromide (DTAB, cationic). Contrast variation SANS studies using deuterated version of $C_{12}EO_6$ or SDS, or by varying the D_2O/H_2O ratio of the suspensions (with CapB), allowed focusing only on the structural properties of OCNF or surfactants micelles. We showed that, in the concentration range studied, $C_{12}EO_6$, although it concentrates the nanofibrils thanks to an excluded volume effect observed in SANS, does not affect the rheological properties of the suspensions. Addition of SDS or CapB induces gelation for surfactant concentrations superior to the critical micellar concentration (CMC). SANS results show that attractive interactions between OCNF arise in the presence of these anionic or zwitterionic surfactants, hinting at depletion attraction as the main mechanism of gelation. Finally, addition of small amounts of DTAB (below the CMC) allows formation of a tough gel by adsorbing onto the OCNF surface.

Introduction

As the most naturally-abundant polymer,[1] cellulose has raised the interest of scientists in order to design eco-compatible materials.[2] In plants, cellulose is found as tightly-packed bundles of fibrils. Strong hydrogen bonds between fibrils maintain a hierarchical organisation preventing their dispersion in aqueous dispersions.[3] The hydrophilicity of cellulose fibrils can be enhanced by chemical modification, such as TEMPO-mediated oxidation.[3, 4] This method consists of the selective oxidation of the glucosyl C6 primary hydroxyl group, using NaOCl and mediated by NaBr and (2,2,6,6-tetramethylpiperidin-1-yl)oxyl (TEMPO). Negatively-charged carboxyl groups are hence introduced on the surface of cellulose fibrils, and water-dispersible oxidised cellulose nanofibrils (OCNF) are obtained. OCNF are characterised by a cross-sectional diameter of typically 5-10 nm and a length ranging from 100 nm to a few µm and exhibit high surface charges (ζ-potential <-30 mV).[4]

OCNF can form hydrogels in aqueous suspensions, with rheological properties highly dependent on the concentration of nanofibrils,[5-7] the pH of the suspension,[8] the temperature,[9] the nature of the solvent[10] or the presence of additives such as salt,[7, 8, 11] polymers[12, 13] or surfactants.[5, 14] For example, addition of 0.1 M NaCl triggers gelation of OCNF.[15] It was shown both theoretically[11] and experimentally[15] that addition of counter-ions to a suspension results in a charge-screening of OCNF, reducing fibril-fibril electrostatic repulsion which in turn encourages their aggregation into a percolated network. Typical rheological fingerprints of OCNF-based hydrogels are the presence of a yield stress (i.e. the stress above which the materials flow), a pronounced shear-thinning behaviour, and frequency-independent elastic and viscous moduli (*G'* and *G''*, respectively) in oscillatory shear experiments performed within the linear viscoelastic regime. Addition of polymers such as carboxymethyl cellulose was also found to induce gelation, thanks to depletion-flocculation mechanisms.[12] Similar rheological behaviours are observed for cellulose nanocrystals (CNC), negatively-charged rod-like nanoparticles that are generally smaller in length when compared to OCNF.[16, 17] The behaviour of these OCNF hydrogels, associated with the biocompatibility of cellulose makes them promising materials for cosmetics,[18] food[19] or health-care applications[20] (among others), for example as rheology modifiers,[19] scaffolds for tissue engineering[21] or drug-delivery carriers.[22, 23]

Among the type of additives that can be added to those hydrogels, surfactants play an important role in a large range of industrial applications. Understanding the effect of surfactant addition to OCNF suspensions and how to exploit such understanding to induce formation of hydrogels is key to design novel soft materials. We previously showed that the addition to a 2wt% OCNF suspension of a negatively-charged surfactant, sodium lauroyl sarcosinate (SLS), commonly used in shampoo formulation thanks to its high capacity to foam, led to the gelation of the suspension (for concentrations of surfactants ranging from 1 to 5 wt%, ca. 30 to 180 mM).[5] *Quennouz et al.* observed a similar behaviour using 8wt% (ca. 175 mM) of sodium lauryl ether sulfate (SLES) to a 0.6 wt% OCNF suspension.[14] Interestingly, however, sodium dodecyl sulfate (SDS) at 4wt% (ca. 145 mM) led to a loss of sample stability. Moreover, the authors showed gelation could be obtained by adding non-ionic surfactant (Triton-X 100 and Pluronic F68) at high concentration (8 wt%, ca. 140 and 10 mM respectively), while even small quantities of dodecyl trimethyl ammonium bromide (DTAB) resulted in an unstable sample. The authors claimed that gelation of OCNF/surfactant mixtures occurred due to the affinity between the cellulose nanofibri surface and surfactants headgroups. Work on cationic surfactants such as C_nTAB with OCNF or CNC showed indeed a clear affinity between the positively charged headgroup and the negatively-charged surface of the nanocellulose.[24, 25] Regarding non-ionic or anionic surfactants, other hypotheses such as depletion-flocculation, where surfactant micelles act as depletants, have also been suggested.[5] Recently, we studied the effect of the shape of ionic surfactant micelles on the rheological properties of OCNF suspensions in saline conditions.[26] We compared spherical, rod-like and worm-like micelles made by mixing cocamidopropyl betaine (CapB) and SLS; cocamidopropylamine oxide (CapOx) and SDS or CapB and SDS respectively. Addition of salt is a requirement to form worm-like micelles when CapB and SDS are used. We showed that in those saline conditions, where a stiff gel is already formed by OCNF aggregation, addition of micelles leads to an increase of $tan\ \delta = G''/G'$, acting as a plasticizer. Moreover, we saw that the addition of worm-like micelles, acting as a secondary entangled network interferes with the OCNF percolated network.

To shed some light on the gelation mechanisms between OCNF and surfactants without salt, we compare in this paper the rheological and structural properties of OCNF mixtures with either a non-ionic (hexaethylene glycol mono-n-dodecyl ether, $C_{12}EO_6$), anionic (SDS), zwitterionic (CapB) or cationic

(DTAB) surfactant. The four surfactants were chosen as they are all composed of the same $C_{12}H_{25}$ hydrophobic tail, with only the nature of the polar head varying. To probe the structural properties of the suspensions, we used small angle neutron scattering techniques (SANS). SANS is a powerful tool to probe structural changes in these multicomponent systems. Indeed, the technique is non-invasive and *in situ*. It not only gives information about the shape and size of the particles in suspension but also on the interactions between particles. Moreover, using neutrons, contrast variation techniques allow focusing either on the scattering from the cellulose nanofibrils or the surfactant aggregates in the mixtures.

Materials and Methods

Sample preparation

OCNF were synthesised via the TEMPO/NaOCl/NaBr oxidation route followed by high-pressure homogenisation, as described previously,[3, 4] using wood pulp as cellulose source, resulting in an 8wt% solid paste in water. We previously measured the degree of oxidation by conductometric titration, found to be 25%.[21, 27, 28] After synthesis, OCNF were purified in order to remove salts and preservatives using several dialysis steps, following a protocol previously described.[10, 15] After purification, the OCNF solution was freeze-dried. Hexaethylene glycol mono-n-dodecyl ether ($C_{12}EO_6$), sodium dodecyl sulphate (SDS) and dodecyltrimethylammonium bromide (DTAB) were purchased from Sigma-Aldrich and used as received. Commercial grade cocamidopropyl betaine (CapB, Crodateric CAB 30-LQ-(MH), 30% aqueous solution, batch No 1189504) was kindly provided by Croda. CapB was then freeze-dried before use. The critical micelle concentration (CMC) at room temperature of each surfactant can be found in the literature: 0.085 mM for $C_{12}EO_6$,[29] 8.20 mM for SDS,[30] 14.6-16.0 mM for DTAB[30] and 0.28 mM for CapB.[31] A stock suspension of OCNF at 2 wt% and stock suspensions of surfactant at 200 mM in de-ionised water (DI, 18.2 MΩ.cm) were prepared and homogenised with a probe ultrasonicator (Vibracell VC300) using a tapered titanium microprobe (6.5 mm diameter) at an intensity of 10 $W \cdot cm^{-2}$ (applied power determined by heat balance), alternating 1 s sonication with a 1 s standby for 2 min. Then, samples were prepared by mixtures of stock suspensions and DI water to reach 1 wt% OCNF and 20, 40, 60 or 80 mM surfactant (SDS and CapB). We note that for DTAB, addition of 20 mM of surfactant induces a phase separation due to fibril-fibril aggregation, hence concentrations of 1, 5 and 10 mM, below the CMC of this surfactant (ca. 15 mM[30]), where the sample is homogeneous, were chosen. Finally, for control, OCNF (1wt%)-$C_{12}EO_6$ suspensions were studied at 1, 5, 10 mM (matching the concentrations used for the DTAB system) and 50 mM (to compare with SDS and CapB). Note that no extra salt was added to those suspensions. Hence, the change of ionic strength is solely dependent on the concentration in ionic surfactant (up to 10 mM for DTAB and 80 mM for SDS/CapB).

For neutron analysis, deuterated version of SDS and $C_{12}EO_6$ (labelled d-SDS and d-$C_{12}EO_6$ in the following; while hydrogenated version of the surfactants will be labelled h-SDS and h-$C_{12}EO_6$), both exhibiting a deuterated carbon tail, were supplied by the ISIS, Deuteration Facility (Rutherford Appleton Laboratory, Didcot, UK). Suspensions of OCNF (1wt%) and surfactant mixtures for neutron measurements were prepared following the protocol described above, using D_2O, H_2O or mixtures depending on the contrast studied. This allowed doing some contrast matching measurements, i.e. match the scattering length density of one of the components (OCNF or surfactant micelles) with the solvent to focus solely on the other component. For SDS, four contrasts were studied: h-SDS in D_2O (where both OCNF and SDS are visible); d-SDS in D_2O (contrast matching of SDS with the solvent to

probe only OCNF in the mixtures), d-SDS in 50%D_2O (contrast matching of OCNF with the solvent to probe only the surfactant micelles) and finally d-SDS in H_2O (a check contrast, where both OCNF and micelles are visible). For $C_{12}EO_6$, due to the limited synergystic effect between OCNF and nonionic micelles, only two contrasts were studied: h-$C_{12}EO_6$ in D_2O (to see both OCNF and surfactant) and d-$C_{12}EO_6$ in D_2O (to focus on the OCNF). For CapB, only a hydrogenated version of the surfactant was accessible, hence measurements were primarily done in D_2O. Nonetheless, to further discriminate OCNF contribution from the one of the micelles, a contrast variation study was made for CapB 40 mM with the following percentage of D_2O in the solvent: 100; 70; 50 (OCNF contrast matching point), 40, 20 (theoretical contrast matching point of CapB) and 0%. Finally, for DTAB, only one sample at 5 mM was studied in neutron in D_2O. For the DTAB sample no contrast matching measurements were performed as the DTAB concentration is under the CMC. Thus, a negligible scattering contribution to the overall scattering pattern is expected from the DTAB. Surfactants (h-SDS, h-$C_{12}EO_6$ and CapB) were also measured in D_2O in absence of OCNF at the same molar concentrations than the mixtures for comparison.

Rheology measurements

Rheological properties of OCNF-surfactants hydrogels and suspensions were measured at room temperature using a stress-controlled rheometer (Discovery HR-3, TA Instruments) equipped with a sandblasted plate–plate geometry (40 mm or 12 mm in diameter depending on the measurements) with a ca. 1 mm gap. The edge of the geometry was covered with a thin layer of mineral oil to prevent evaporation of water. First, amplitude strain sweep measurements of the storage and loss moduli G' and G'' were conducted at ω = 10 rad.s^{-1}, to assess the amplitude of the linear viscoelastic region. Then, a strain amplitude of 0.1% was chosen for frequency sweep measurements to characterise the possible gel-like behaviour of the suspensions. Finally, steady flow measurements were performed to study the viscosity response of the sample to shearing, with a shear rate $\dot{\gamma}$ ranging from 10^{-2} to 10^{2} s^{-1}.

Small angle neutron scattering (SANS)

Structural properties of the hydrogels were studied using SANS at the Larmor beamline at the ISIS Pulsed Neutron and Muon Source at the Rutherford Appleton Laboratory (RAL, Didcot, UK).[32] A typical q-range of $4.5\text{x}10^{-3} \leq q \leq 0.7$ Å^{-1}, with q the scattering vector, was chosen. Measurements associated with the $C_{12}EO_6$ system were carried out at the Sans2D beamline at RAL.[33] In all cases, sample were poured into 1 cm wide, 1 mm thick neutron cells and measured at room temperature. From the raw data, background subtraction and normalisation of the scattering intensity were conducted using the Mantid software to give the scattered intensity *I(q)* in absolute scaling (cm^{-1}).[34]

SANS data treatment

SANS data were fitted using a home-made Fortran software, via a least-squared fitting procedure. For isotropic suspensions, the normalised scattered intensity *I(q)* can be described as follows:[35]

$$I(q) = I_{scatterers}(q) + B = AP(q)S(q) + B$$

with $I_{scatterers}(q) = AP(q)S(q)$ the contribution from the scattering objects, $A = n\Delta\rho^2V^2 = \varphi_p\Delta\rho^2V$ the scaling factor depending on the number of scatterers per unit volume n in cm^{-3} or the volume fraction of particles in the sample φ_p, the contrast between the scatterers and the solvent $\Delta\rho = \rho_s - \rho_0$ (ρ_s and ρ_0 the scattering length densities of the scatterers and solvents respectively in

cm^{-2}) and *V* the volume of the scatterers (in cm^3), *P(q)* the normalised form factor of the scatterers (*P(q=0)*=1) and *S(q)* the structure factor of the scatterers. *B* is a constant background parameter in cm^{-1}.

For OCNF, previous studies have shown they could be described as rod-like particles, either with a parallelepiped or elliptical cross-section.[15, 36] We selected the elliptical cross-section model to fit the data. We previously demonstrated that the intensity associated with OCNF, $I_{scatterers}(q) = I_{OCNF}(q)$, can be written:[15]

$$I_{OCNF}(q) = A_{OCNF} P_{rod}(q, R_{max}, \varepsilon, L) S_{PRISM}(q, \nu_{RPA}, R_{Cq})$$

with A_{OCNF} the scaling factor associated with OCNF, $P_{rod}(q,R_{max},\varepsilon,L)$ the form factor for rods with a length L ≥100 nm (not measurable in the given q-range and later fixed at 160 nm as determined by transmission electron microscopy in our previous study[15]) and a cross-section described by the larger radius R_{max} (in nm) and ellipticity $\varepsilon<1$; and $S_{PRISM}(q,\nu_{RPA},R_{Cq})$ the structure factor for rods using the PRISM model,[37] with ν_{RPA} representing the strength of the interactions between rod-like particles ($\nu_{RPA}<0$ for attractive interactions, $\nu_{RPA}>0$ for repulsive interactions), and R_{Cq} the radius of excluded volume along each point of the rod. The complete description of this model can be found in ref [15] and is not repeated here.

Similarly, the intensity associated with micelles of surfactants, $I_{scatterers}(q) = I_{micelles}(q)$, can be written as:

$$I_{micelles}(q) = A_{micelles} P_{micelles}(q) S_{micelles}(q)$$

with $A_{micelles}$ the scaling factor of the micelles, $P_{micelles}(q)=P_{spheres}(q,R,\sigma)$ the form factor of polydisperse spheres of radius R (in nm) and polydispersity index σ (in %) valid for micelles of SDS or CapB. For micelles of $C_{12}EO_6$, an elliptical model is preferred with $P_{micelles}(q)=P_{ellipses}(q,R,\varepsilon_p)$ the form factor of ellipsoids of dimensions $(R,R,\varepsilon_p R)$ with radius R and ε_p the ellipticity parameter ($\varepsilon_p>1$ for prolate-type ellipsoids). The complete model description can be found in ref [38]. Structure factors used for sphere and ellipsoid-like micelles depend on the type of interactions between micelles (steric or electrostatic).

For the non-ionic $C_{12}EO_6$ micelles and the zwitterionic CapB micelles, a hard-sphere model is enough to describe the interactions between micelles. The hard-sphere potential of interaction can be written as:

$$V(r) = \begin{cases} \infty, & r \leq R_{HS} \\ 0, & r > R_{HS} \end{cases}$$

with r the distance from the particle centre, R_{HS} the hard-sphere radius of interaction ($R_{HS}>R$). The associated structure factor was calculated by Percus and Yevick.[39] $S_{micelles}(q)=S_{Percus\text{-}Yevick}(q,R_{HS},\varphi_{HS})$, depends not only on R_{HS} the hard-sphere radius of interactions but also φ_{HS} the volume fraction of interacting micelles.[38]

For the negatively-charged SDS micelles, coulomb interaction has to be taken into account in the form of a Coulomb or Yukawa potential:[40]

$$V(r) = \begin{cases} \infty, & r \leq R \\ \dfrac{U}{r} e^{-\kappa r}, & r > R \end{cases}$$

with *r* the distance from the particle centre. Analytical versions of the structure factor were given by Hayter and Penfold via the mean spherical approximation,[41] or the Yukawa structure factor.[40] The Yukawa structure factor can be written as: $S_{micelles}=S_{Yukawa}(q,R,\varphi,U,1/\kappa)$ with *R* the radius of the particles, φ the volume fraction of interacting particles, *U* the strength of the Coulomb interaction and $1/\kappa$ the Debye-Hückel length characterising the length of electrostatic interaction.[40] We note that Hayter and Penfold have shown previously that for dilute micellar solution, the mean spherical approximation structure factor leads to unphysical results. A similar issue is observed with the Yukawa structure factor. This problem is circumvented by defining an effective radius $R_{eff}>>R$ for the interacting particles, which reaches a volume fraction of interaction φ_{eff} large enough to properly fit the data.[42] This rescaled mean sphere approximation structure factor hence gives R_{eff}, φ_{eff} and $(1/\kappa)_{eff}$. By denoting $x=R/R_{eff}$ the rescaling factor, the real values of these dimensions are given by $\varphi=\varphi_{eff}x^3$ and $(1/\kappa)=x(1/\kappa)_{eff}$. Note that in the solution provided by Hayter and Penfold, the surface charge on the micelles is extracted using the dielectric permittivity of the solvent and the salt concentration of the suspension.[40]

For mixtures of OCNF and micelles, we have simply summed both contributions, neglecting possible cross-term in the calculation of the scattered intensity.

$$I(q) = I_{OCNF}(q) + I_{micelles}(q) + B$$

This simplification is enough to describe the data and evidence whether interactions arising between OCNF and micelles are present.

Results

Mixtures of OCNF and $C_{12}EO_6$

We first studied the addition of $C_{12}EO_6$ to a 1wt% OCNF suspension. In our conditions, a 1wt% OCNF suspension (in the absence of surfactants) presents a fluid-like behaviour at rest (i.e., in the limit of small amplitudes in a classical oscillatory experiment), while gelation is only observed for concentrations ≥ 2wt%.[15] The concentration of gelation is highly dependent of the type of OCNF used, and notably their overall dimensions.[5, 7, 14] $C_{12}EO_6$ was chosen as non-ionic surfactant to see if addition of non-electrostatically interacting micelles can influence the rheological properties at the probed concentrations (1 to 50 mM, above the CMC of the surfactant of 0.085 mM[29]), purely due to the excluded volume effect. This will help decorrelate the further effect of the charge of the micelles for the other systems.

Figure 1.a presents the viscosity curves of suspensions made of OCNF at 1wt%, without or with different concentrations of $C_{12}EO_6$. The presence of micelles of $C_{12}EO_6$ has little influence on the viscosity of the suspension, neither acting as a thickening nor thinning agent. At all concentrations, suspensions exhibit a shear thinning behaviour already observed for OCNF-based suspensions and hydrogels.[5] Moreover, the suspensions still present a fluid-like behaviour ($G''>G'$), as observed in the frequency and amplitude sweeps in **Figure S1** in Supplementary Information; with an important angular dependency of both G' and G'' in the frequency sweeps (**Figure S1.a**) and a large linear viscoelastic region (**Figure S1.b**). These results suggest that at those concentrations, the addition of micelles of $C_{12}EO_6$ has little influence on the overall rheological properties of the sample, which are instead governed by the cellulose nanofibrils.

Structural information can be obtained using small angle neutron scattering (SANS). **Figure S2** in Supplementary Information gives the SANS pattern of an OCNF suspension at 1wt%, the fit associated and the parameters from the fitting procedure. The SANS pattern is characteristic of rod-like structures, with a broad signal at large angles from the elliptical cross-section, and a q^{-1} behaviour (seen as a -1 slope in log-log scale) at small angles. Interactions would induce a deviation from this q^{-1} behaviour (a less pronounced slope would be associated with repulsion between fibrils, a more pronounced one with attraction). OCNF can hence be fitted as fibrils of length fixed at 160 nm, in agreement with previous work[15] (as it is not accessible in the probed q-range) with an elliptical cross-section of maximum radius R_{max}=5.0±0.1 nm and ellipticity ε=0.22±0.01. This model corresponds well to previous TEM and cryo-TEM measurements of the nanofibrils.[15] At this concentration, no interaction between fibrils is required to fit the data (ν_{RPA}=0). The results are consistent with previous SAXS and SANS studies.[15, 43]

SANS patterns of $C_{12}EO_6$ micelles in D_2O are provided in **Figure S3**. They can be fitted using a model of prolate ellipsoids of radius R and ellipticity ε_p>1. The higher the concentration of surfactant, the more anisotropic the ellipsoids become while keeping R constant. Hence, in this case, the change of shape with concentration induces an increase of the volume of the micelle $V = \frac{4}{3}\pi\varepsilon_p R^3$, that goes from 96.7 nm^3 at 1 mM to 260.0 nm^3 at 50 mM. The highest concentration (50 mM) was even fitted using interactions between micelles via the Percus-Yevick model for hard spheres. Fit parameters are given in **Table 1**. This behaviour is consistent with previous SANS studies of $C_{12}EO_6$ micelles in solution.[44]

Table 1 – Fitting parameters of the SANS patterns for solutions of $C_{12}EO_6$ micelles at different concentration.

[$C_{12}EO_6$] (mM)	**1**	**5**	**10**	**50**
$A_{micelles}$ /±0.01 cm^{-1}	0.15	0.85	1.82	19.08
R /±0.1 nm	2.4	2.4	2.4	2.4
ε_p /±0.02	1.67	1.95	2.06	4.49
R_{HS} (nm) /±0.1 nm	-	-	-	3.9
ϕ /±0.5 %	-	-	-	5.8

Figure 1.b and 1.c gives the SANS patterns for mixtures of OCNF and $C_{12}EO_6$, using either a deuterated version of the surfactant (d-$C_{12}EO_6$) to focus on OCNF or a hydrogenated version of the surfactant (h-$C_{12}EO_6$) to study both OCNF and micelles. Using d-$C_{12}EO_6$ (partial deuteration as only the carbon tail is deuterated), we can fit the data using the signal of OCNF nanofibrils only for [d-$C_{12}EO_6$]≤10 mM (see **Figure 1.b**, and **Table 2** for the main parameters extracted from of the fits). For 1 and 5 mM, the dimensions of the nanofibrils are fixed according to results from the SANS pattern of OCNF at 1wt%. At 5 mM, we need to add repulsive interactions between nanofibrils: with ν_{RPA}=2.66±0.01 the strength of the repulsion and R_{Cq}=R_{max}=*5.0* nm (fixed during the fitting) the excluded volume radius around the fibril cross-section. For 10 mM, we have also to adjust slightly the nanofibril dimensions (R_{max}=4.1±0.1 nm and ε=0.44±0.02), while maintaining repulsion between nanofibrils (ν_{RPA}=1.76±0.01 and R_{cq}=8.6±0.1 nm). We explain this apparent change in nanofibril cross-section by the rise of an extra contribution from the d-$C_{12}EO_6$ micelles in the SANS pattern, neglected during fitting. Indeed, as the polar head is not deuterated, the micelles are not exactly contrast matched with the solvent, hence the micelles shell can still contribute to the SANS pattern, especially in the q-range associated with the nanofibrils cross-section. This is easily seen at 50 mM, where several oscillations are observed at q≥0.05 $Å^{-1}$. The signal cannot be fitted using the model of rod-like nanofibrils. This SANS pattern is

probably the sum of nanofibrils and shell-contrasted micelles. Due to the complexity of this system, fitting was not attempted.

When OCNF and h-$C_{12}EO_6$ are mixed (**Figure 1.c**), the SANS patterns can be fitted well by simply summing the contributions of OCNF and $C_{12}EO_6$, without any change in either the micelle or the fibril form factors. The only adjustable parameters are the scaling factors of both OCNF and micelles contributions (A_{OCNF} and $A_{micelles}$ respectively) and the fibril interaction parameters (ν_{RPA} and R_{Cq}), which all can be found in **Table 2**. We note that adding repulsion between nanofibrils has an effect only at the smallest angles, as can be seen in **Figure S4** which compares the fits obtained for OCNF+h-$C_{12}EO_6$ at 50 mM with and without repulsion between nanofibrils. Reasonable fits can already be obtained without repulsion for all concentrations, but the presence of repulsion when d-$C_{12}EO_6$ is used and smaller values for the least-square fitting parameter χ^2 (which estimates the deviation between the experimental scattering intensity and the fitted intensity in each data point, see S.I.) when repulsion is added (4.33 versus 4.99 for 50 mM) indicate that repulsive interactions between nanofibrils must be accounted for. The values of $A_{micelles}$ and A_{OCNF} are not affected by the addition of a repulsive structure factor between nanofibrils. Further, the values of $A_{micelles}$ found in the mixtures are of the same order of magnitude as for the samples without OCNF at the same concentration, while A_{OCNF} strongly increases with the micelle concentration. A similar trend for A_{OCNF} is observed for the samples with d-$C_{12}EO_6$ (see **Table 2**).

This behaviour is unexpected as the scaling factor depends on the number of OCNF per unit volume and the contrasts, both parameters expected to be unchanged by the addition of surfactants. For comparison, OCNF at 2 wt% without surfactant was also measured in SANS (see **Figure S5** for the SANS patterns and fitting parameters), and the scaling factor is found to be $A_{OCNF}=(1.5\pm0.1)\times10^{-2}$ cm^{-1} at this nanofibril concentration (ca. $2.34\times A_{OCNF\ at\ 1wt\%}$). Results with OCNF 1wt% and 10 mM h-$C_{12}EO_6$ hence give the same order of magnitude for A_{OCNF}. And in both cases, OCNF experience repulsion ($\nu_{RPA}=1.62\pm0.01$ for the system OCNF 2 wt%, >2 for OCNF + $C_{12}EO_6$ as shown in **Table 2**). These results suggest that adding $C_{12}EO_6$ may result in concentrating the nanofibrils in the water phase due to an excluded volume effect. The change in scale would hence be an increase of the apparent crowding of OCNF, with adding 10 mM of $C_{12}EO_6$ being roughly equivalent to double the concentration of nanofibrils. A similar effect of suspension crowding was previously investigated with CNC in the presence of polymer. It was shown that adding polymer had the same effect on the alignment of CNC under shear as self-crowding induced by increasing the concentration, notably, on the value of the shear rate for the onset of particle alignment.[45]

Nonetheless, we showed in a previous work that increasing the concentration of nanofibrils from 1 to 2 wt% in aqueous solutions results in a liquid-to-gel phase transition observed in rheology, that we attributed to the emergence of repulsive electrostatic interactions between nanofibrils seen in small angle x-ray scattering.[15] Similarly, SANS fitting of the suspension of OCNF at 1wt% alone does not require the addition of interactions between nanofibrils ($\nu_{RPA}=0$) while repulsive interactions ($\nu_{RPA}=1.62\pm0.01$ and $R_{Cq}=R_{max}=5.0$ nm) are needed at 2 wt% (see **Figures S2** and **S5**). Yet, in mixtures of OCNF and $C_{12}EO_6$, we see an emergence of repulsive interactions between nanofibrils, consistent with the increase in nanofibril crowding by excluded volume effect, but no gel is observed in rheology. An interesting feature is the excluded radius around the nanofibrils cross-section R_{Cq}. For nanofibrils alone (OCNF at 2wt%), R_{Cq} is fixed at R_{max} the radius of the nanofibrils. Letting free this parameter only results in that case in its decrease, yet, by definition $R_{Cq}\geq R_{max}$ (the excluded volume radius cannot be smaller

than the particle radius). Similarly, when micelles are "contrast matched" (OCNF 1wt% + d-$C_{12}EO_6$), we observe the same results. This indicates that indeed, the presence of micelles induces a concentration of the nanofibrils that hence experience repulsion. Nonetheless, when micelles are "visible" (OCNF 1wt% + h-$C_{12}EO_6$), although repulsion between nanofibrils is present, we find $R_{Cq}>>R_{max}$, which suggests that micelles also act as a steric barrier between nanofibrils, disturbing the overall network and preventing gelation from occurring macroscopically. A crude geometrical calculation supports this theory. Defining $x=R_{Cq}-R_{max}$, one can note that for 5 mM x=5.3 nm ≈ 2R=4.8 nm with R the radius of the micelles. The increase of x with micelle concentration could be related to the elongation of the micelles.

Interestingly, previous work from *Quennouz et al.* showed that gelation of OCNF suspensions could be obtained by adding non-ionic surfactants, in their case Triton-X or Pluronic F68.[14] They required a large amount of surfactant (1 wt%) to see a mild increase of the rheological properties of the hydrogels. We can hypothesise that those surfactants induce gelation by concentrating OCNF in the water phase, in a similar fashion as $C_{12}EO_6$ here seen in SANS or even by acting as depletants to induce gelation by depletion-flocculation; but that they do not disturb the OCNF network as strongly as $C_{12}EO_6$ micelles do. Indeed, Triton X-100 and Pluronic F68 are known to form oblate[46] and spherical[47] micelles respectively. It is then possible that the shape variation of $C_{12}EO_6$ micelles with concentration is what is preventing gelation in our system. Indeed, we saw previously that having elongated micelles can more efficiently disturb the OCNF network.[26] Moreover, we also showed that the OCNF network integrity could really be affected by the presence of nanofillers with a size larger than the mesh size of the network.[48] Both phenomena may explain the incapacity of $C_{12}EO_6$ to induce gelation by depletion forces or simply by crowding.

Table 2 – Fitting scaling factors for suspensions of OCNF at 1wt%, h-$C_{12}EO_6$ at 1; 5; 10 or 50 mM and mixtures (OCNF+h-$C_{12}EO_6$ and OCNF+d-$C_{12}EO_6$). For OCNF+h$C_{12}EO_6$, the data were fitted using the sum of the two contributions; where the scaling factors and fibril-fibril interactions were the only adjustable parameters (with the background term, not shown). For OCNF+d-$C_{12}EO_6$, the data were fitted with the signal of OCNF only for [d-$C_{12}EO_6$]≤10 mM. The error is ±0.01 cm^{-1} for $A_{micelles}$, ±0.01 x10^{-2} cm^{-1} for A_{OCNF}, ±0.01 for v_{RPA} and ±0.1 nm for R_{Cq}. x is a calculated parameter obtained from R_{Cq} and R_{max} after fitting. Parameters *in italic* were fixed during fitting, while / signals an unnecessary parameter.

	[$C_{12}EO_6$] (mM)	0	1	5	10	50
OCNF 1wt%	A_{OCNF} /x10^{-2} cm^{-1}	0.64	/	/	/	/
$C_{12}EO_6$	$A_{micelles}$ /cm^{-1}	/	0.15	0.85	1.82	19.08
OCNF + h-$C_{12}EO_6$	A_{OCNF} /x10^{-2} cm^{-1}	/	0.55	0.76	1.24	3.78
	$A_{micelles}$ /cm^{-1}	/	0.14	0.63	1.29	13.76
	v_{RPA} / no unit	*0*	*0*	2.56	3.60	2.29
	R_{Cq} / nm	/	/	10.3	12.5	17.9
	$X=R_{Cq}-R_{max}$ / nm	/	/	5.3	7.7	12.9
OCNF + d-$C_{12}EO_6$	A_{OCNF} /x10^{-2} cm^{-1}	/	0.66	0.75	0.90	/
	v_{RPA} / no unit	*0*	*0*	2.26	1.76	/
	R_{Cq} / nm	/	/	*5.0*	8.6	/

Hence, we can conclude that addition of $C_{12}EO_6$ at relatively low concentration (<100 mM) is enough to influence the crowding of OCNF in suspension thanks to excluded volume effect, but that it has little influence on the overall suspension rheological properties, probably as it also acts as steric barriers between nanofibrils.

Mixtures of OCNF and SDS

As OCNF are negatively charged particles, the addition of a charged surfactant may have a larger influence on the properties of the suspension. We hence studied the addition of SDS to the system.

Figure 2 gives the rheological properties of mixtures of OCNF at 1wt% and SDS at various concentrations. Contrarily to $C_{12}EO_6$, the addition of this anionic surfactant has a clear effect on the rheological properties of the suspensions; which are forming hydrogels. Indeed, they exhibit an increased viscosity (**Figure 2.a**), a dominant gel-like behaviour with *G'>G''* over a wide frequency range (**Figure 2.b**) and a large linear viscoelastic regime (**Figure 2.c**). The gel-like behaviour is characterised by *G'>G''*, and a modest frequency dependency even for the highest SDS concentrations indicates a weak physical gel. Importantly, with the increase of SDS concentration, the *G'* and *G''* dependency as a function of angular frequency (ω) flattens out, indicating the slowing down of OCNF dynamics due to the presence of SDS. A similar trend was observed by *Quennouz et al.* with SLES.[14] Hence, the addition of SDS triggers the liquid-to-gel phase transition while maintaining relatively low shear viscosity and storage modulus compared to other methods of gelation. Indeed $\eta(\dot{\gamma} = 0.1)$ reaches ca. 40 Pa.s for the mixture of OCNF 1wt% with [SDS]=80 mM, while it is >100 Pa.s for a suspension of OCNF at 2 wt%, see ref [15]. Similarly, *G'(ω=1)=2* Pa for OCNF(1wt%)+SDS(80mM), but reaches 70 Pa for OCNF(2wt%).

As salt is known to induce gelation by charge screening of the nanofibrils, it is interesting to consider the influence of the ionic surfactant on the ionic strength *I* of the suspension. It could help determine whether the gelation is related to the presence of more counterions in the solution that would screen the surface charges of OCNF. The variation of ionic strength is directly related to the concentration of SDS within the sample. It can be written:[49]

$$I \approx CMC + \frac{\alpha}{2}(c - CMC)$$

With *c* the concentration of SDS in mM, CMC its critical micellar concentration (8.2 mM) and *α*=0.567 the degree of micelle ionisation.[49] For *c*=20 mM, the increase in ionic strength is hence *I*=11.5 mM while it reaches *I*=28.6 mM at *c*=80 mM. For comparison, a gel-like behaviour was clearly observed for OCNF at 1wt% and [NaCl]=0.1M only (i.e. a ionic strength of 100 mM).[15] Hence, gelation in presence of SDS is triggered at much lower ionic strength than in presence of NaCl.

A second hypothesis is that the addition of SDS may alter the pH of the solution, which in turn could drastically change the ζ-potential of OCNF nanofibrils. pH measurements of SDS suspensions showed little variation as a function of pH (pH=6.6 at *c*=0 mM, 6.0 at *c*=20 mM and 6.0 at *c*=80 mM). We previously showed that OCNF exhibit a clear stable ζ-potential of *ca.* -60 mV for pH≥4.[50] This invalidates this hypothesis.

Moreover, the absence of yield strain on the amplitude sweeps (see **Figure 2.c**), even at strains reaching 100 %, suggests a homogeneous microstructure with a network that can withstand large deformations. This behaviour is different from the attractive colloidal gel behaviour observed when the charges between nanofibrils are screened by the addition of salt or the change of pH.[15, 50]

A fine study of SANS data of both pure SDS micelles and mixtures of OCNF and SDS can help unravel the mechanisms of gelation between the negatively charged nanofibrils and the anionic micelles (see

Figure 3). The SANS patterns for SDS micelles alone (red curves in **Figure 3**) are characteristic of interacting spherical objects, with an oscillation at ca. q=0.1 Å^{-1} associated with the size of the objects, and a broad peak at ca. q=0.05 Å^{-1}, increasing with micelles concentration, due to the electrostatic repulsion between micelles. At 80 mM, the increase observed at small angles is probably an artefact from the subtraction. The patterns can be fitted using the model of charged spheres presented in Material and Methods. Fitting of the micelle dimensions were made with the sample at 40 mM to have a clear signal-to-noise ratio; then the radius was fixed for all other concentrations, with only the interaction parameters adjustable. Micelles are characterised by their radius R=1.8±0.1 nm and their polydispersity σ=11±1% at 20 mM or 17±1% (for the other concentrations). Miura et al evidenced a second cmc via conductivity measurements at 65 mM, usually associated with micelle elongation.[51] Nonetheless, as satisfactory fits were obtained with spherical micelles even at 80 mM, we privileged this simpler model. Fitting of the micelle-micelle interactions was made using the Yukawa structure factor. **Table 3** gives the values of U, φ and $(1/\kappa)$ the strength of interaction, the volume fraction of interacting micelles and the Debye-Hückel length of interaction, respectively.

Table 3 – Scaling factor and parameters associated to the structure factor from the fits of SDS micelles at different concentrations. The parameters associated with the form factor of the spherical micelles, R=1.8±0.1 nm and σ=11±1% (20 mM) or 17±1% (40 mM and above), were adjusted at 20 and 40 mM and then were fixed at the other concentrations.

[SDS] (mM)	20	40	60	80
$A_{micelles}$ /±0.01 cm^{-1}	0.29	0.95	1.47	1.59
ϕ ±0.02%	0.54	0.83	1.11	1.48
(1/κ) /±0.1 Å	32.8	11.8	7.8	8.5
U /±0.1	1.3	1.6	1.7	1.8

An increase in the micelle concentration is associated with an expected increase of φ, the volume fraction of interacting micelles, and a decrease of the Debye-Hückel length $(1/\kappa)$, consistent with a reduced inter-micellar distance; while the overall potential of repulsion, U, slightly increases.

Regarding mixtures of OCNF at 1wt% and SDS micelles, the contrast made using d-SDS and D_2O (green curves in **Figure 3**) allows studying only the nanofibrils. Contrarily to the signal of OCNF 1wt% alone, this time the slope deviates strongly from the q^{-1} behaviour, with a much more pronounced slope, indicating attraction between fibrils. Indeed, they were fitted using the same OCNF form factor as previously, but all concentrations required the addition of an attractive structure factor (ν_{RPA}<0). No clear tendency regarding the strength of the attraction can be drawn from the SANS fits though, as both samples made with 20 and 60 mM SDS exhibit an unusually high attraction ($\nu_{RPA}\leq$-5), while suspensions at 40 and 80 mM present a "weaker" attraction (-2≤$\nu_{RPA}\leq$-1).

Another contrast made using d-SDS in 50% D_2O (blue curves on **Figure 3**) focuses only on SDS micelles. The signal resembles the one of pure SDS micelles, but it can be clearly observed that the strength of micellar repulsion is lowered in the mixture, with a broader peak found at larger angles compared to the system made purely of SDS. Specifically, the Debye-Hückel length of interaction $(1/\kappa)$ is strongly reduced in the mixed systems (from 11.8 to 5.6 with the addition of OCNF for [SDS]=40 mM) as seen in. Hence, similarly to the nanofibril, the micelle-micelle electrostatic repulsion is lowered in the mixtures.

Table 4 – Parameters associated to the structure factor from the fits of OCNF 1wt% +SDS micelles at different concentrations using the contrast d-SDS in 50%D_2O. At this contrast, the contribution from OCNF nanofibril is removed.

[SDS] (mM)	20	40	60	80
ϕ ±0.02%	0.36	0.89	1.27	1.61
(1/κ) /±0.1 Å	13.2	5.6	3.8	2.6
U /±0.1	1.5	1.2	1.3	1.5

The last 2 contrasts, (yellow and pink curves in **Figure 3**) can be fitted by summing the contribution of both attractive OCNF and SDS micelles, fixing both nanofibrils and micelles form factor parameters. Nonetheless, while we could fit the data by fixing the strength of nanofibrils attraction according to the results found at the contrast d-SDS/D_2O, we had to make the micelle interaction parameters adjustable for each contrast to have a satisfactory fitting of the data. These differences are probably the signature of nanofibril-micelle interactions that are neglected in our fitting model. **Table 5** gives the results of the fits for the system OCNF+SDS at 40 mM and for all contrasts; while **Tables S1, S2** and **S3** in supplementary information give the results for 20; 60 and 80 mM respectively. The variation of scaling factors with contrasts can be easily explained by the differences in deuterium/hydrogen ratios, as $A \propto \Delta\rho^2$, with $\Delta\rho$ the SLD contrast between scatterers (nanofibrils or micelles) and solvents. We note that for the last two contrasts, the signal from micelles is highly dominating the SANS patterns, and it would not be possible to extract the fibril structure factor solely from those two contributions. Actually, satisfactory fits of those two contrasts can already be obtained assuming v_{RPA}=0 (no interactions between nanofibrils). Nonetheless, as the contrast using d-SDS in 50% D_2O, focusing only on OCNF, proves without a doubt that attractive interactions between nanofibrils are at play, we decided to keep this attractive interactions contribution for the contrasts h-SDS in D_2O and d-SDS in H_2O, where both OCNF and micelles are visible.

Analysis of SANS data reveals that in mixtures of nanofibrils and SDS micelles, OCNF experiences attractive interactions, while the overall repulsion between micelles is reduced. Moreover, results also hint at the presence of nanofibril-micelle interactions. A similar behaviour was previously observed by Kline and Kaler when studying mixtures of Ludox silica spheres and SDS.[52] Also in their case, the essentially non-interacting Ludox spheres experienced attraction in presence of SDS, while the screened Coulomb repulsion between micelles is reduced. The authors attributed these results to depletion attraction of Ludox spheres by the presence of the SDS micelles and vice-versa; while the Ludox-SDS interaction is probably related to steric/electrostatic repulsion. Associated with the difference in size between nanofibrils (length > 100 nm) and micelles (typically 1-2 nm in radius), the presence of attraction between nanofibrils may hint at depletion-flocculation as the main mechanism for the gel formation. Nonetheless, this mechanism would give an attractive colloidal gel which contradicts the amplitude sweep measurements discussed earlier. A more nuanced view is that the gelation is probably due to a balance between nanofibril-nanofibril depletion attraction and nanofibril-micelle electrostatic repulsion that tune the depletion-induced gelation mechanism, resulting in a more stable microstructure. This may explain why the gel properties are highly sensitive to the amount of SDS added, and notably why Quennouz et al. observed a loss of stability at high SDS concentration due to fibril aggregation.[14]

Our measurements were carried out in the absence of salt to probe only the effect of SDS micelles on the hydrogels. As salt and anionic surfactant induce gelation via seemingly different mechanisms, it

would be interesting to probe a hydrogel in presence of anionic surfactant and salt. Previous work carried out on a mixture of OCNF at 1wt% and N-laurylsarcosine sodium salt (SLS), another anionic surfactant, in presence of 1wt% NaCl, showed weaker values of *G'* and *G''* when the surfactant was added than in its absence.[26] This suggests that the gelation mechanism triggered by anionic surfactants and the OCNF charge screening in the presence of salt are competitive phenomena. Moreover, the addition of salt can also influence the micelles by notably screening their Coulomb repulsion. A hypothesis is that in presence of salt, charge screening of OCNF induces the formation of a stiff network that is the main mechanism for gelation in that case, while anionic micelles act solely as steric barriers disturbing this attractive colloidal network. This could be further studied in the future.

Table 5 – Scaling factors and structure factors parameters obtained from the fits of the SANS data for mixtures of OCNF 1wt% + SDS 40 mM at different contrasts. The form factor parameters for both OCNF and micelles were fixed according to the values found for each separate system. Parameters in italic were fixed during fitting, while / indicates that this parameter was not required.

contrast	d-SDS/D_2O	d-SDS/50%D_2O	h-SDS/D_2O	d-SDS/H_2O
A_{OCNF} /(±0.01)x10^{-2} cm^{-1}	0.73	/	0.40	0.21
$A_{micelles}$ /±0.01cm^{-1}	/	0.48	0.99	1.21
v_{RPA}	-1.37	/	*-1.37*	*-1.37*
ϕ ±0.03%	/	0.89	0.34	*0.34*
(1/κ) /±0.1 Å	/	5.6	0.6	*0.6*
U /±0.1	/	1.2	*1.2*	*1.2*

Mixtures of OCNF and DTAB

Due to the positive charge of the polar head, DTAB is expected to strongly interact with the negatively-charged nanofibrils. And indeed, even at concentrations below the CMC, addition of DTAB to a 1wt% OCNF suspension results in a stiff gel, as evidenced by **Figure 4.a, b and c**.

High viscosities (with a viscosity at 10^{-2} s^{-1} in the range of 1000 Pa.s) and storage and loss moduli (with values almost 100 times higher than for samples made with SDS at 80 mM) are observed for the samples containing DTAB. Moreover, the frequency sweeps show little frequency dependency, indicating that the OCNF are in an arrested state within the probed time frame (i.e., $1/\omega$). The strain required for the material to yield is usually defined in amplitude sweep measurements by the point in strain at which *G'=G''*. We note that for the samples containing DTAB (especially at 10 mM), *G'* decreases and approaches the value of *G''*. Thus, the amplitude sweeps indicate the approaching of yielding of the gel due to the dislodging of the nanofibrils composing the network. Contrarily, for the OCNF+SDS samples, *G'* does not converge towards *G''* within the probed strains, indicating that larger values of strains are required for the material to yield.

The elasticity (captured by *G'*) and viscosity of the samples containing DTAB at concentrations of 5 and 10 mM are superior to those obtained for a suspension of OCNF at 1wt% with 100 mM NaCl,[15] although in the latter a higher amount of positive charges were added. This strongly indicates that not only the charged polar head but also the hydrophobic tail of the surfactant has an influence on the macroscopic properties. A possible mechanism of gelation could be the adsorption of the polar head of the surfactant onto the nanofibrils surface due to electrostatic attraction. This would render the nanofibril not only less charged, but also more hydrophobic; which could encourage fibril-fibril aggregation

between "hydrophobic patches" of two nanofibrils. We hence monitored in SANS the system at 5 mM of DTAB (see **Figure 4.d**). Interestingly, the systems exhibit a SANS pattern largely modified compared to the signal of pure OCNF at 1wt%. To simulate fibril side-side aggregation, we fitted this pattern using a signal of fibrils with the same length L fixed at 160 nm but a larger cross-section with a radius R_{max}=32.0±0.1 nm and ε=0.11±0.02 (much larger than the typical dimensions of OCNF). Moreover, a small oscillation at q=0.15 Å^{-1} requires the addition of a signal from small spheres of radius R=1.5±0.1 nm to be fitted. This may indicate that some DTAB micelles are present, although we are expected to be below the CMC (i.e., ~3× below the CMC).[30] Great caution should be taken from the actual values of the fit, or even the model chosen to describe the data, which may be inadequate. Nonetheless, it is still clear that when DTAB is added, OCNF fibrils experience strong charge screening and aggregation explaining the rheological properties observed.

Furthermore, the system is highly sensitive to the amount of DTAB added, as 1 mM is not enough to trigger this aggregation phenomenon, while too large amounts of DTAB (20 mM and above) result in macroscopic phase separation; in agreement with previous work from *Quennouz et al*.[14]

Mixtures of OCNF and CapB

Finally, CapB was chosen as it is composed of the same C_{12} hydrophobic tail as the other surfactants studied, but its betaine polar head exhibits both positive (thanks to the quaternary ammonium group) and negative charges (via the final carboxylic group). This zwitterionic surfactant also strongly influences the rheological properties of OCNF suspensions, as seen in **Figure 5**. The viscosity of the suspensions are of the same order of magnitude as for mixtures of OCNF and SDS, with a shear viscosity at 0.1 s^{-1} of ca. 10-50 Pa.s for the highest surfactant amounts (60 and 80 mM, see **Figure 5.a**). A fluid-to-gel phase transition is also observed with increasing concentration of surfactant. Interestingly, the gel properties at 80 mM of CapB are ca. 10 times higher than for its SDS counterpart (see **Figures 5.b** and **2.b** respectively), with a weaker frequency dependency. Similarly to the samples with SDS, yielding of the gel is not observed in the probed strains in the amplitude sweeps, although a deviation from the linear viscoelastic regime is observed for G' and G" at ca. 50 and 30% for concentration of 60 mM and 80 mM respectively (**Figure 5.c**). Moreover, similarly again to anionic surfactants, we showed in a previous publication that the addition of CapB to a OCNF suspension in presence of salt leads to a reduction of both G' and G'', suggesting that when a stiff network is formed, CapB micelles act also like a steric barrier.[26]

Similarly to SDS, we can calculate the increase in ionic strength with surfactant concentration (with α=0.88 for CapB).[53] For the CapB concentration c=20 mM, the increase in ionic strength is I=9 mM and reaches I=35.4 mM at c=80 mM. They are hence of the same order of magnitude as when SDS is used. Again, pH measurements showed no effect of the addition of CapB to the pH (with values of 6.6 at c=20 mM and 6.4 at c=80 mM).

From the rheological properties, we can hypothesise that similar gelation mechanisms between OCNF and CapB are at play when compared with SDS. Nonetheless, the presence of positive charges within the polar head might be responsible for the much higher storage and loss moduli of the samples compared to the system with SDS. This hypothesis is again verified using SANS data. **Figure 6** gives the SANS patterns of pure CapB suspensions (**Figure 6.a**) and mixtures of OCNF and CapB (**Figure 6.b**) in D_2O. As we only have access to a hydrogenated version of the surfactant, we did some contrast variation studies at [CapB]=40 mM by varying the D_2O/H_2O composition of the solvent (**Figure 6.c**).

At all concentrations, CapB micelles can be fitted as spheres of radius R=2.4±0.1 nm and polydispersity σ=15-17%. To properly model the signal at small angles, weak steric repulsion between micelles, modelled using the Percus-Yievick structure factor, must be taken into account for concentrations ≥40 mM. The results from the fits are given in **Table 6**.

Surprisingly, for mixtures of OCNF and CapB (with the exception of the sample at 40 mM), the SANS data can satisfactorily be fitted by simply summing the contributions from micelles and nanofibrils, without further interactions between nanofibrils or nanofibrils and micelles. Moreover, except for the sample at 80 mM, the scaling factors A_{OCNF} and $A_{micelles}$ are found to be similar in these mixtures compared to suspensions containing only OCNF or CapB micelles (see **Table 7**). At 80 mM, the signal of OCNF seems weaker than expected (A_{OCNF}=(0.41±0.01)x10^{-2} cm^{-1} versus (0.64±0.01)x10^{-2} cm^{-1} for a suspension of OCNF at 1wt% only), which may be explained by the dominance of the signal from micelles at this concentration. This is a striking difference compared to the case with non-ionic $C_{12}EO_6$ where A_{OCNF} increased with concentration. We note that the $C_{12}EO_6$ micelles present a much lower CMC (0.085 mM versus 0.28 mM) and undergo a clear change of shape with concentration (from quasi spherical to highly elongated). We expect elongated objects to more drastically affect the OCNF network[26] and hence concentrate the nanofibrils. On the contrary, CapB micelles remain spherical at all concentration, with an occupied volume fraction below 3% as seen from the fitting of pure micelle suspensions (see **Table 6**). This should explain why the overall volume fraction occupied by nanofibrils (and hence the scaling factor A_{OCNF}) is unaltered by the micelles' presence.

Table 6 - Fitting parameters to model the SANS patterns of CapB micelles in D_2O at different concentrations (SANS patterns can be found in Figure 7). Parameters *in italic* were fixed during the fitting procedure, while parameters marked with / were not needed.

[CapB] / mM	20	40	60	80
$A_{micelles}$ /±0.01 cm^{-1}	1.00	1.94	3.04	4.07
R /±0.1 nm	2.4	*2.4*	*2.4*	*2.4*
σ /±1 %	17	15	*15*	*15*
R_{HS} /±0.1 nm	/	4.2	3.7	3.3
ϕ /±0.2 %	/	1.0	1.9	2.6

Table 7 - Fitting scaling factors for suspensions of OCNF at 1wt%, CapB at 20; 40; 60 or 80 mM and mixtures (Mix). In that last case, the data were fitted using the sum of the two contributions; where the scaling factors were the only adjustable parameters. The error is ±0.01 cm^{-1} for $A_{micelles}$ and ±0.01 x10^{-2} cm^{-1} for A_{OCNF}.

	[CapB] (mM)	0	20	40	60	80
OCNF 1wt%	A_{OCNF} /x10^{-2} cm^{-1}	0.64	/	/	/	/
CapB	$A_{micelles}$ /cm^{-1}	/	1.00	1.94	3.04	4.07
Mix	A_{OCNF} /x10^{-2} cm^{-1}	/	0.73	0.59	0.63	0.41
	$A_{micelles}$ /cm^{-1}	/	1.04	2.07	3.19	4.22

As previously pinpointed, no evidence of attraction between nanofibrils (contrarily to the mixtures with SDS) is seen from the SANS data, except possibly for the sample at 40 mM where a slight increase is seen at the smallest angles (cyan curve in **Figure 6.b**). As already demonstrated with the other surfactants, contrast matching studies are crucial to isolate the contribution from OCNF, especially at high surfactant concentrations. Hence, we studied OCNF 1wt% + CapB 40 mM at different D_2O/H_2O ratios for the solvent (see **Figure 6.c**). 20 % D_2O (pink curve) corresponds to the matching point of CapB

micelles. The data were fitted using attraction between nanofibrils, with v_{RPA}=-3.10±0.01 and R_{Cq} fixed at R_{max}. Then, all the other contrasts can be fitted summing the contributions of CapB micelles and attractive fibrils. Nonetheless, contrarily to SDS, no extra contribution or alteration of OCNF/CapB structure factor, that would be associated with nanofibril-micelle interactions (neglected in our model) is required to give a satisfactory fit of the data. Scaling parameters are given in **Table S4**, SI.

The evidence of fibril-fibril attraction with the contrast variation studies suggests that, as with SDS, the fibrils evidence a slight depletion attraction in presence of CapB. The CapB structure factor seems unaffected by the presence of OCNF, nonetheless one must remember interactions between CapB are modelled with only a very weak hard-sphere potential instead of a strong coulomb repulsion with SDS. The absence of nanofibril-micelle interactions here is more puzzling but may be related to the absence of net charge for the micelles. The absence of such nanofibril-micelle strong repulsion (that is expected to oppose the rising depletion attraction between nanofibrils) would explain the higher values of *G'* and *G''* for samples with CapB than SDS at the same concentration but also the deviation from the linear viscoelastic regime observed in the amplitude sweeps at the highest CapB concentrations. Hence, these results suggest that mixtures of OCNF and CapB exhibit similar gelation mechanisms as those containing OCNF and SDS. It is highly possible that OCNF in suspensions with 60 and 80 mM CapB experience fibril attraction as well, but due to the strength of the signal of micelles in pure D_2O, this is not detected in this contrast. For 20 mM, the signal from OCNF is still clearly high compared to the contribution of the micelles, with a q^{-1} slope visible at small angle, which suggests that attraction between nanofibrils is not present or quite weak at this concentration. Further contrast studies, preferentially with a deuterated version of the surfactant to avoid a strong incoherent scattering signal from hydrogens would help ensure that the results observed at 40 mM can be applied to the other concentrations.

Conclusion

In this work, we studied the effect on OCNF suspensions of surfactants bearing a $C_{12}H_{25}$ tail and either a non-ionic ($C_{12}EO_6$), anionic (SDS), cationic (DTAB) or zwitterionic (CapB) polar head. We compared the rheological properties of these OCNF-surfactants suspensions with their structural properties measured in SANS. We showed the type of polar head had a strong influence on the properties of the suspensions, namely with gelation induced when the polar head exhibits charges. Indeed, we showed that, at the concentrations probed, the non-ionic surfactant does not affect the rheological properties of a 1wt% OCNF suspension, which exhibit a fluid-like behaviour. SANS results suggest that if non-ionic micelles induces crowding of OCNF in the water phase due to an excluded volume effect, they also act as steric barrier between nanofibrils preventing gelation. Their change in shape with concentration, going from quasi-spherical to elongated micelles might prevent them to act as depletants. On the contrary, addition of SDS induces a fluid-to-gel phase transition, with a weak physical gel behaviour observed in rheology. SANS measurements made at different contrasts show that nanofibrils exhibit attraction in the presence of SDS, while electrostatic repulsion between micelles decreases. Moreover, results suggest a nanofibril-micelle interaction is also arising. These results hint at a competition between depletion attraction and steric stabilisation as the main force driving gelation. Similarly, CapB also induces gelation, with slightly tougher gels compared to SDS when added at the same concentration. SANS data for the sample at 40 mM hint at depletion-induced gelation, notably as fibril-fibril attraction is evidenced while no fibril-micelle interaction is observed. Results at other concentrations are less clear and future measurements using contrast matching techniques would help

confirm this result. Finally, DTAB had the strongest effect on the dispersion, with tough and stiff gels obtained at concentrations below the CMC (5 and 10 mM). SANS data suggest fibril aggregation, probably as DTAB adsorbs at the surface of the nanofibrils to screen the negative charges, making them more hydrophobic. At higher concentrations of DTAB, the gels obtained are unstable and phase separation occurs. Understanding the nature of the interactions between OCNF and surfactants is a key step in the use of these bio-based materials for commercial applications.

Supplementary Material

See supplementary material for the definition of χ^2 in SANS fitting, rheological data for OCNF (1wt%) + $C_{12}EO_6$, SANS data for individual components OCNF, $C_{12}EO_6$, and their mixtures, and the fitting parameters for OCNF with SDS and CapB.

Acknowledgements

The authors thank EPSRC for funding this project (grant EP/N033310/1). Dr Vincenzo Calabrese thanks the University of Bath for PhD studentship funding. Experiments at the ISIS Pulsed Neutron and Muon Source were supported by beam time allocations for Larmor from the Science and Technology Facilities Council under proposal number RB1720220. Measurements on $C_{12}EO_6$ systems were made on Sans 2D (proposal number RB1720206). All data supporting this paper are openly available from the University of Bath data archive at: XXXXXX.

References

1. Klemm, D.; Heublein, B.; Fink, H.-P.; Bohn, A., Cellulose: Fascinating Biopolymer and Sustainable Raw Material. *Angew. Chem. Int. Ed.* **2005,** *44*, 3358 – 3393.
2. Johnson, R. K.; Zink-Sharp, A.; Renneckar, S. H.; Glasser, W. G., A new bio-based nanocomposite: fibrillated TEMPO-oxidized celluloses in hydroxypropylcellulose matrix. *Cellulose* **2009,** *16*, 227–238.
3. Saito, T.; Nishiyama, Y.; Putaux, J.-L.; Vignon, M.; Isogai, A., Homogeneous Suspensions of Individualized Microfibrils from TEMPO-Catalyzed Oxidation of Native Cellulose. *Biomacromolecules* **2006,** *7* (6), 1687-1691.
4. Isogai, A.; Saito, T.; Fukuzumi, H., TEMPO-oxidized cellulose nanofibers. *Nanoscale* **2011,** *3*, 71-85.
5. Crawford, R. J.; Edler, K. J.; Lindhoud, S.; Scott, J. L.; Unali, G., Formation of shear thinning gels from partially oxidised cellulose nanofibrils. *Green Chem.* **2012,** *14*, 300-303.
6. Nechyporchuk, O.; Naceur Belgacem, M.; Pignon, F., Concentration effect of TEMPO-oxidized nanofibrillated cellulose aquous suspensions on the flow instabilities and small-angle X-ray scattering structural characterization. *Cellulose* **2015,** *22*, 2197-2210.
7. Geng, L.; Peng, X.; Zhan, C.; Naderi, A.; Sharma, P. R.; Mao, Y.; Hsiao, B. S., Structure characterization of cellulose nanofiber hydrogel as functions of concentration and ionic strength. *Cellulose* **2017,** *24*, 5417-5429.
8. Fall, A. B.; Lindstrom, S. B.; Sundman, O.; Odberg, L.; Wagberg, L., Colloidal Stability of Aqueous Nanofibrillated Cellulose Dispersions. *Langmuir* **2011,** *27*, 11332–11338.
9. Calabrese, V.; Munoz-Garcia, J.; Schmitt, J.; Da Silva, M. A.; Scott, J. L.; Angulo, J.; Khimyak, Y. Z.; Edler, K. J., Understanding heat-driven gelation of anionic cellulose nanofibrils: combining STD NMR, SAXS and rheology. *Journal of Colloid and Interface Science* **2019,** *535*, 205-2013.
10. da Silva, M. A.; Calabrese, V.; Schmitt, J.; Celebi, D.; Scott, J. L.; Edler, K. J., Alcohol induced gelation of TEMPO-oxidized cellulose nanofibril dispersions. *Soft Matter* **2018,** *14*, 9243-9249.

11. Fukuzumi, H.; Tanaka, R.; Saito, T.; Isogai, A., Dispersion stability and aggregation behavior of TEMPO-oxidized cellulose nanofibrils in water as a function of salt addition. *Cellulose* **2014,** *21*, 1553-1559.
12. Ferreira Souza, S.; Mariano, M.; de Farias, M. A.; Silva Bernardes, J., Effect of depletion forces on the morphological structure of carboxymethyl cellulose and micro/nano cellulose fiber suspensions. *Journal of Colloid and Interface Science* **2019,** *538*, 228-236.
13. Hossen, M. R.; Dadoo, N.; Holomakoff, D. G.; Co, A.; Gramlich, W. M.; Mason, M. D., Wet stable and mechanically robust cellulose nanofibrils (CNF) based hydrogels. *Polymer* **2018,** *151*, 231-241.
14. Quennouz, N.; Hashmi, S. M.; Choi, H. S.; Kim, J. W.; Osuji, C. O., Rheology of cellulose nanofibrils in the presence of surfactants. *Soft Matter* **2016,** *12*, 157-164.
15. Schmitt, J.; Calabrese, V.; Da Silva, M. A.; Lindhoud, S.; Alfredsson, V.; Scott, J. L.; Edler, K. J., TEMPO-oxidised cellulose nanofibrils; probing the mechanisms of gelation via Small Angle X-Ray Scattering. *Phys .Chem. Chem. Phys.* **2018,** *20*, 16012-16020.
16. Heline Lopes da Fonseca, J.; Akira d'Avila, M., Rheological behavior of carboxymethylcellulose and cellulose nanocrystal aqueous dispersions. *Rheologica Acta* **2021,** *60*, 497-509.
17. Oguzlu, H.; Boluk, Y., Interactions between cellulose nanocrystals and anionic and neutral polymers in aqueous solutions. *Cellulose* **2017,** *24*, 131-146.
18. Meftahi, A.; Samyn, P.; Abbasi Geravand, S.; Khajavi, R.; Alibkhshi, S.; Bechelany, M.; Barhoum, A., Nanocelluloses as skin biocompatible materials for skincare, cosmetics, and healthcare: Formulations, regulations, and emerging applications. *Carbohydrate Polymers* **2022,** *278*, 118956.
19. Aaen, R.; Simon, S.; Wernersson Brodin, F.; Syverud, K., The potential of TEMPO-oxidized cellulose nanofibrils as rheology modifiers in food systems. *Cellulose* **2019,** *26*, 5483-5496.
20. Califano, D.; Lee Patenall, B.; Kadowaki, M. A. S.; Mattia, D.; Scott, J. L.; Edler, K. J., Enzyme-Functionalized Cellulose Beads as a Promising Antimicrobial Material. *Biomacromolecules* **2021,** *22*, 754-762.
21. Courtenay, J. C.; Johns, M. A.; Galembeck, F.; Deneke, C.; Lanzoni, E. M.; Costa, C. A.; Scott, J. L.; Sharma, R. I., Surface modified cellulose scaffolds for tissue engineering. *Cellulose* **2017,** *24* (1), 253-267.
22. Abeer, M. M.; Amin, M. C. I. M.; Martin, C., A review of bacterial cellulose-based drug delivery systems: their biochemistry, current approaches and future prospects. *J. Pharm. Pharmacol* **2014,** *66*, 1047–1061.
23. Celebi, D.; Guy, R. H.; Edler, K. J.; Scott, J. L., Ibuprofen delivery into and through the skin from novel oxidized cellulose-based gels and conventional topical formulations. *Int. J. Pharm* **2016,** *514*, 238–243.
24. Xhanari, K.; Syverud, K.; Chinga-Carrasco, G.; Paso, K.; Stenius, P., Reduction of water wettability of nanofibrillated cellulose by adsorption of cationic surfactants. *Cellulose* **2011,** *18*, 257-270.
25. Brinatti, C.; Huang, J.; Berry, R. M.; Tam, K. C.; Loh, W., Structural and Energetic Studies on the Interaction of Cationic Surfactants and Cellulose Nanocrystals. *Langmuir* **2016,** *32*, 689-698.
26. Da Silva, M. A.; Calabrese, V.; Schmitt, J.; Hossain, K. M. Z.; Bryant, S. J.; Mahmoudi, N.; Scott, J. L.; Edler, K. J., Impact of wormlike micelles on nano and macroscopic structure of TEMPO-oxidized cellulose nanofibril hydrogels. *Soft Matter* **2020,** *16*, 4887-4896.
27. Johns, M. A.; Bernardes, A.; Ribeiro De Azevedo, E.; Guimaraes, F. E. G.; Lowe, J. P.; Gale, E. M.; Polikarpov, I.; Scott, J. L.; Sharma, R. I., On the subtle tuneability of cellulose hydrogels: implications for binding of biomolecules demonstrated for CBM 1. *J. Mater. Chem. B* **2017,** *5*, 3879-3887.
28. Habibi, Y.; Chanzy, H.; Vignon, M. R., TEMPO-mediated surface oxidation of cellulose whiskers. *Cellulose* **2006,** *13*, 679 –687.
29. Di, A.; Schmitt, J.; Ma, K.; Da Silva, M. A.; Elstone, N. S.; Mahmoudi, N.; Li, P.; Washington, A.; Wang, Z.; Errington, R. J.; Edler, K. J., Antagonistic mixing in micelles of amphiphilic

polyoxometalates and hexaethylene glycol monododecyl ether. *Journal of Colloid and Interface Science* **2020,** *578*, 608-618.
30. Aguiar, J.; Carpena, P.; Molina-Bolivar, J. A.; Carnero Ruiz, C., On the determination of the critical micelle concentration by the pyrene 1:3 ratio method. *Journal of Colloid and Interface Science* **2003,** *258*, 116-122.
31. Staszak, K.; Wieczorek, D.; Michocka, K., Effect of Sodium Chloride on the Surface and Wetting Properties of Aqueous Solutions of Cocamidopropyl Betaine. *J. Surfact. Deterg.* **2015,** *18*, 321-328.
32. Bennington, S. M., Instruments on the ISIS second target station. *Nuclear Instruments and Methods in Physics Research Section A: Accelerators, Spectrometers, Detectors and Associated Equipment* **2008,** *600* (1), 32-34.
33. Heenan, R. K.; Rogers, S. E.; Turner, D.; Terry, A. E.; Treadgold, J.; King, S. M., Small Angle Neutron Scattering Unsing Sans2d. *Neutron News* **2011,** *22* (2), 19-21.
34. http://www.mantidproject.org/ISIS_SANS ISIS SANS Data Reduction in Mantid.
35. Pedersen, J. S., Modelling of Small-Angle Scattering Data from Colloids and Polymer Systems. In *Neutrons, X-Rays and Light*, Zemb, T.; Lindner, P., Eds. Elsevier Science: 2002.
36. Mao, Y.; Liu, K.; Zhan, C.; Geng, L.; Chu, B.; Hsiao, B. S., Characterization of Nanocellulose Using Small-Angle Neutron, X-ray, and Dynamic Light Scattering Techniques. *J. Phys. Chem. B* **2017,** *121*, 1340−1351.
37. Schweizer, K. S.; Curro, J. G., PRISM Theory of the Structure, Thermodynamics, and Phase Transitions of Polymer Liquids and Alloys. *Adv. Polym. Sci.* **1994,** *116*, 319-377.
38. Pedersen, J. S., Analysis of small-angle scattering data from colloids and polymer solutions: modeling and least-squares fitting. *Advances in Colloid and Interface Science* **1997,** *70*, 171-210.
39. Percus, J. K.; Yevick, G. J., Analysis of Classical Statistical Mechanics by Means of Collective Coordinates. *The Physical Review* **1958,** *110*, 1-13.
40. Wu, C.; Chan, D. Y. C.; Tabor, R. F., A simple and accurate method for calculation of the structure factor of interacting charged spheres. *Journal of Colloid and Interface Science* **2014,** *426*, 80-82.
41. Hayter, J. B.; Penfold, J., An analytic structure factor for macroion solutions. *Molecular Physics* **1981,** *42* (1), 109-118.
42. Hansen, J.-P.; Hayter, J. B., A rescaled MSA structure factor for dilute charged colloidal dispersions. *Molecular Physics* **1982,** *46* (3), 651-656.
43. Courtenay, J. C.; Jin, Y.; Schmitt, J.; Hossain, K. M. Z.; Mahmoudi, N.; Edler, K. J.; Scott, J. L., Salt-Responsive Pickering Emulsions Stabilized by Functionalized Cellulose Nanofibrils. *Langmuir* **2021,** *37*, 6864-6873.
44. Gapinski, J.; Szymanski, J.; Wilk, A.; Kohlbrecher, J.; Patkowski, A.; Holyst, R., Size and Shape of Micelles Studied by Means of SANS, PCS, and FCS. *Langmuir* **2010,** *26* (12), 9304-9314.
45. Calabrese, V.; Varchanis, S.; Haward, S. J.; Shen, A. Q., Alignment of Colloidal Rods in Crowded Environments. *Macromolecules* **2022,** *55*, 5610−5620.
46. Paradies, H., Shape and size of a nonionic surfactant micelle. Triton X-100 in aqueous solution. *Jurnal of Physical Chemistry* **1980,** *84* (6), 599-607.
47. Costanzo, S.; Di Sarno, A.; D'Apuzzo, M.; Avallone, P. R.; Raccone, E.; Bellissimo, A.; Auriemma, F.; Grizzuti, N.; Pasquino, R., Rheology and morphology of Pluronic F68 in water. *Physics of Fluids* **2021,** *33*, 043113.
48. Calabrese, V.; da Silva, M. A.; Porcar, L.; Bryant, S. J.; Hossain, K. M. Z.; Scott, J. L.; Edler, K. J., Filler size effect in an attractive fibrillated network: a structural and rheological perspective. *Soft Matter* **2020,** *16*, 3303.
49. Danov, K. D.; Basheva, E. S.; Kralchevsky, P. A.; Ananthapadmanabhan, K. P.; Lips, A., The metastable states of foam films containing electrically charged micelles or particles: Experiment and quantitative interpretation. *Advances in Colloid and Interface Science* **2011,** *168* 50–70.
50. Calabrese, V.; da Silva, M. A.; Schmitt, J.; Munoz-Garcia, J.; Gabrielli, V.; Scott, J. L.; Angulo, J.; Khimyak, Y.; Edler, K. J., Surfactant controlled zwitterionic cellulose nanofibril dispersions. *Soft Matter* **2018,** *14*, 7793-7800.

51. Miura, M.; Kodama, M., The second CMC of the aqueous solution of Sodium Dodecyl Sulfate. I. Conductivity. *Bulletin of the Chemical Society of Japan* **1972,** *45*, 428-431.
52. Kline, S. R.; Kaler, E. W., Interactions in binary mixtures: Partial structure factors in mixtures of sodium dodecyl sulfate micelles and colloidal silica. *J. Chem. Phys.* **1996,** *105*, 3813.
53. El-Dossoki, F. I.; Abdalla, N. S. Y.; Gomaa, E. A.; Hamza, O. K., An insight into thermodynamic and association behaviours of cocamidopropyl betaine (CAPB) surfactant in water and water–alcohol mixed media. *SN Applied Sciences* **2020,** *2*, 690.

Figure Captions

Figure 1 – (a) Shear viscosity of OCNF (1wt%) + $C_{12}EO_6$ (0, 1, 5, 10 or 50 mM) suspensions. (b,c) SANS patterns of mixtures of OCNF (1wt%) + $C_{12}EO_6$ in D_2O, using either a tail-deuterated (b) or hydrogenated (c) version of the surfactant. In both cases, concentrations of surfactant studied were 1; 5; 10 and 50 mM. The fits, made by (b) the model of rod-like repulsive nanofibrils with an elliptical cross-section and (c) the sum of the model of uncharged prolate ellipsoidal micelles and rod-like repulsive nanofibrils are provided as black lines.

Figure 2 - Rheological data for OCNF (1wt%) + SDS (0, 20, 40, 60 and 80 mM, see colour code in inset of (a)) suspensions: (a) Shear viscosity, (b) oscillatory frequency sweeps and (c) amplitude sweeps. For (b) and (c), *G'* is given as solid symbols and *G''* as open symbols.

Figure 3 - SANS patterns of pure SDS micelles in D_2O associated with mixtures at different contrasts of OCNF (1wt%) + SDS at (a) 20 mM, (b) 40 mM, (c) 60 mM and (d) 80 mM. The fits made using the model of charged spherical micelles (for pure SDS) and sum of attractive nanorods and charged spherical micelles (for mixtures) are provided as black lines.

Figure 4 – (a, b, c) Rheological data for OCNF (1wt%) + DTAB (0, 1, 5 and 10 mM, see colour code in inset of (a)) suspensions: (a) Shear viscosity, (b) oscillatory frequency sweeps and (c) amplitude sweeps. For (b) and (c), *G'* is given as solid symbols and *G''* as open symbols. (d) SANS pattern of OCNF 1wt% + DTAB 5 mM in D_2O. In black the fit made using fibril-like objects is given.

Figure 5 - Rheological data for OCNF (1wt%) + CapB (0, 20, 40, 60 and 80 mM, see colour code in inset of (a)) suspensions: (a) Shear viscosity, (b) oscillatory frequency sweeps and (c) amplitude sweeps. For (b) and (c), *G'* is given as solid symbols and *G''* as open symbols.

Figure 6 - SANS patterns of (a) suspensions of CapB in D_2O and (b) mixtures of OCNF (1wt%) + CapB in D_2O. In both cases, concentrations of surfactant studied were 20; 40; 60 and 80 mM. (c) SANS patterns of the mixture OCNF (1wt%) and CapB (40 mM) for different D_2O/H_2O compositions. The fits, made by (a) the model of uncharged spherical micelles or (b, c) the sum of nanorods and uncharged spherical micelles are provided as black lines.

a)

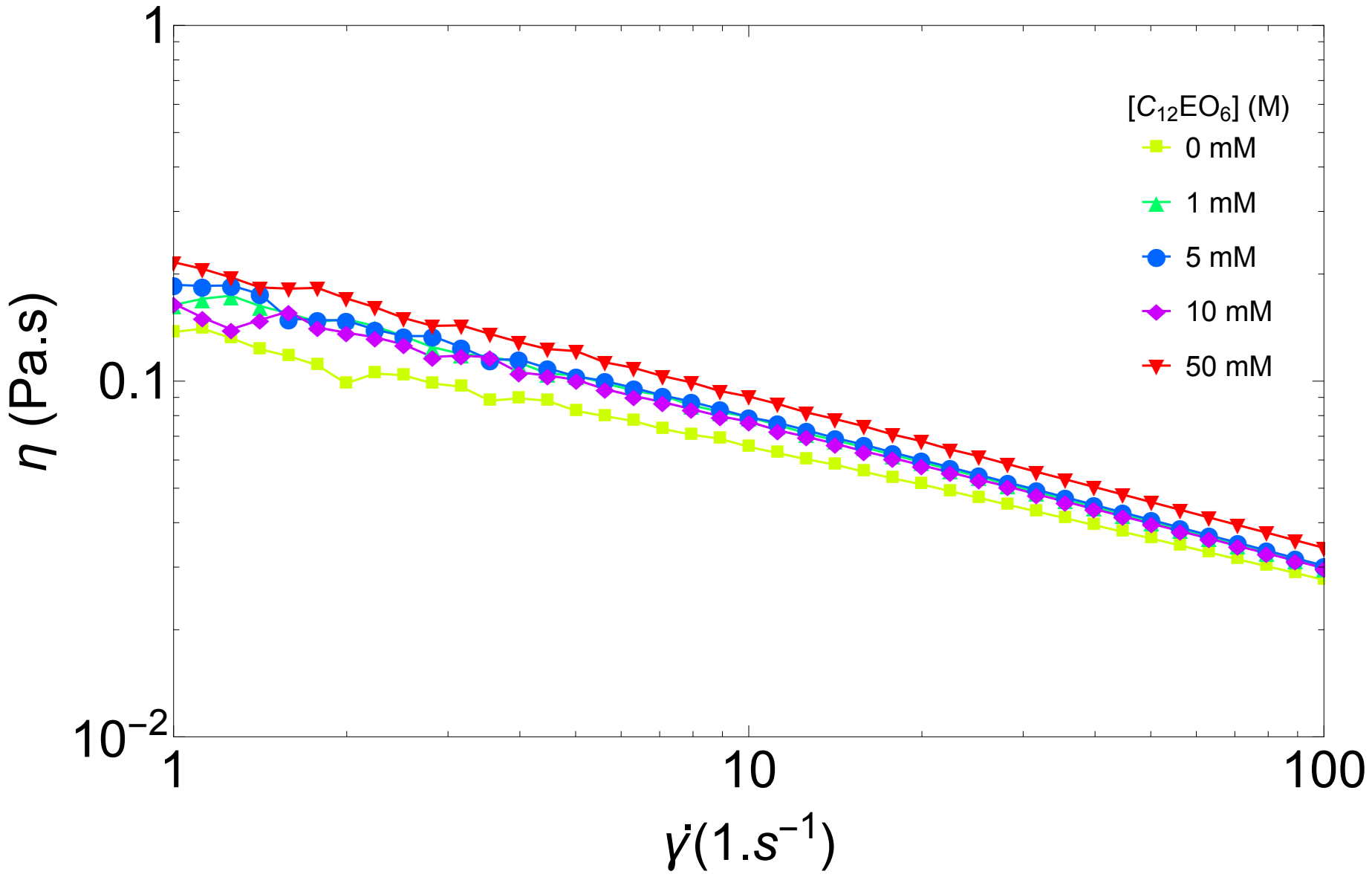
1
0.1
10^{-2}
η (Pa.s)
1
10
100
$\dot{\gamma}(1.s^{-1})$
[$C_{12}EO_6$] (M)
0 mM
1 mM
5 mM
10 mM
50 mM

b)

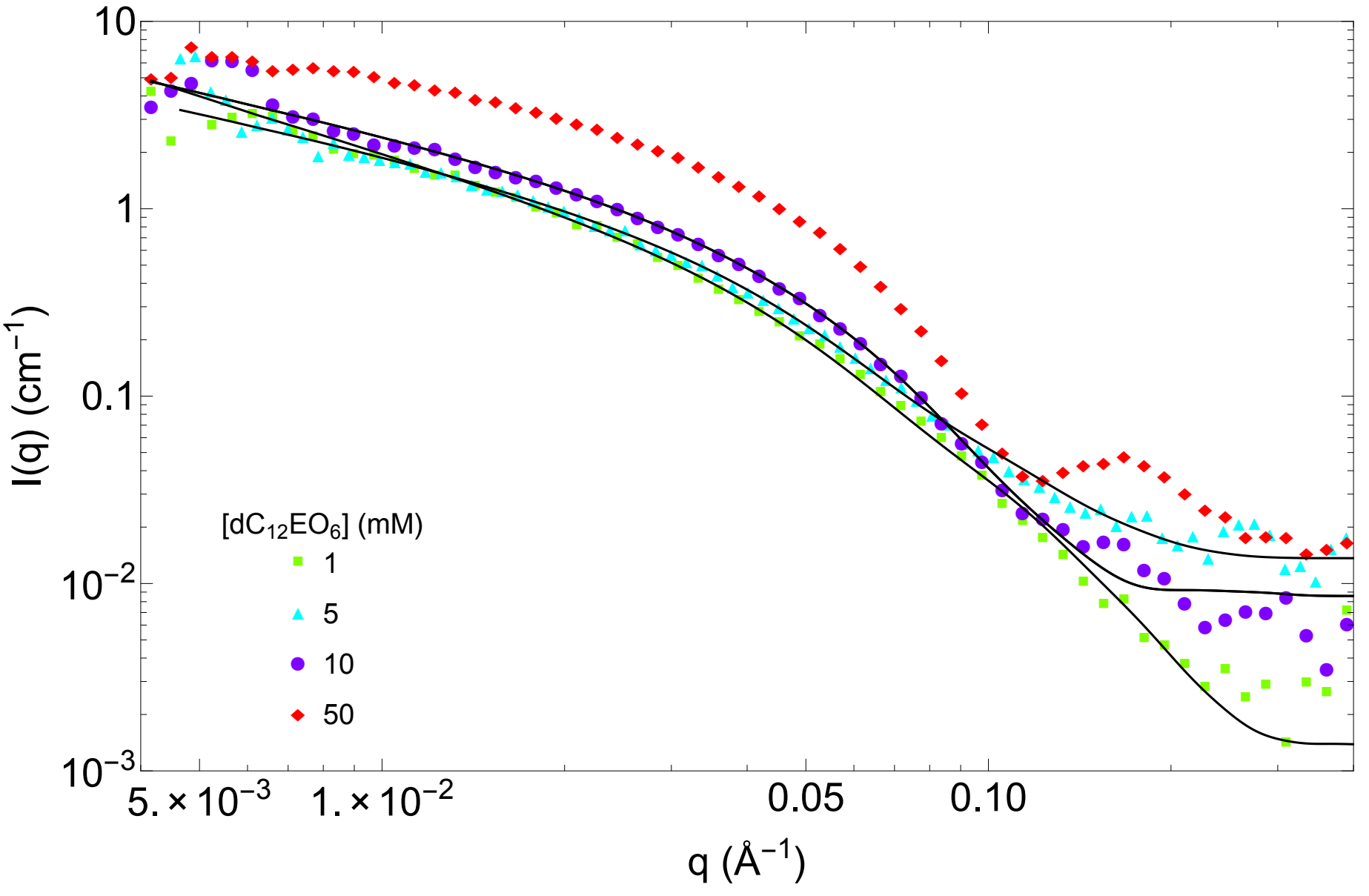
10
1
0.1
10^{-2}
10^{-3}
I(q) (cm^{-1})
$5.\times10^{-3}$
$1.\times10^{-2}$
0.05
0.10
q ($Å^{-1}$)
[$dC_{12}EO_6$] (mM)
1
5
10
50

c)

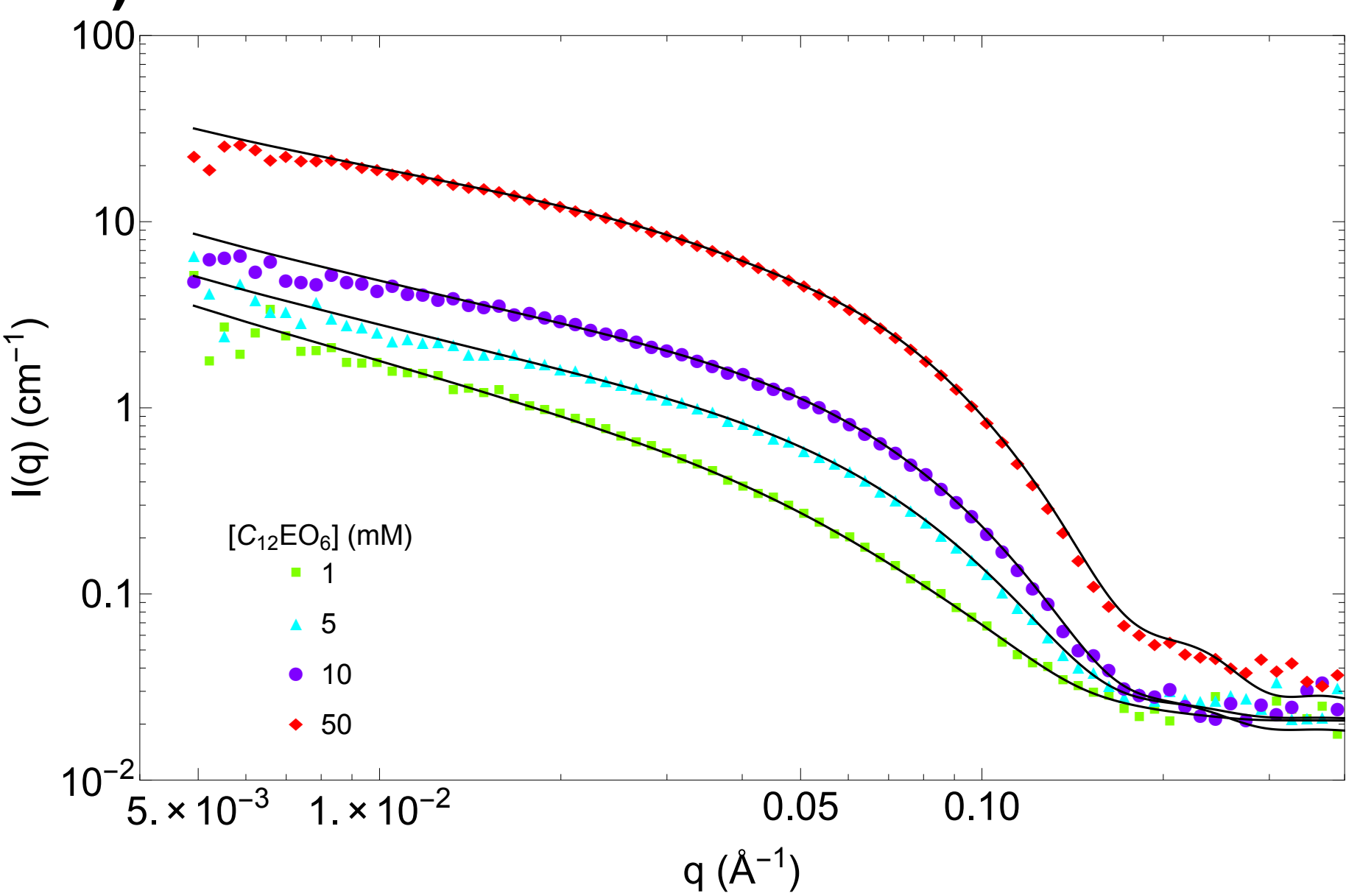
100
10
1
0.1
10^{-2}
I(q) (cm^{-1})
$5.\times10^{-3}$
$1.\times10^{-2}$
0.05
0.10
q ($Å^{-1}$)
[$C_{12}EO_6$] (mM)
1
5
10
50

a)

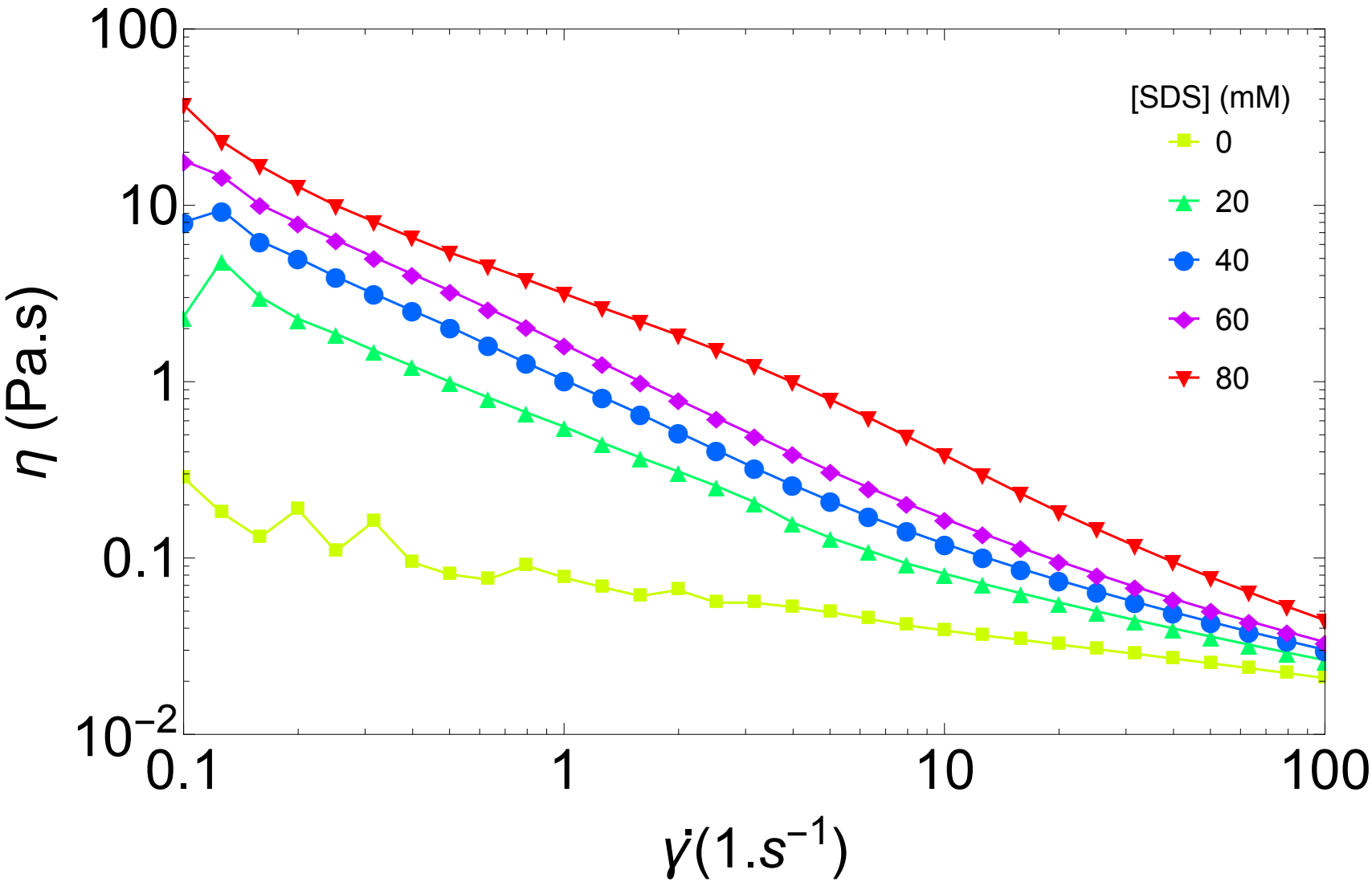
100
10
1
0.1
10^{-2}
0.1
1
10
100
η (Pa.s)
$\dot{\gamma}(1.s^{-1})$
[SDS] (mM)
0
20
40
60
80

b)

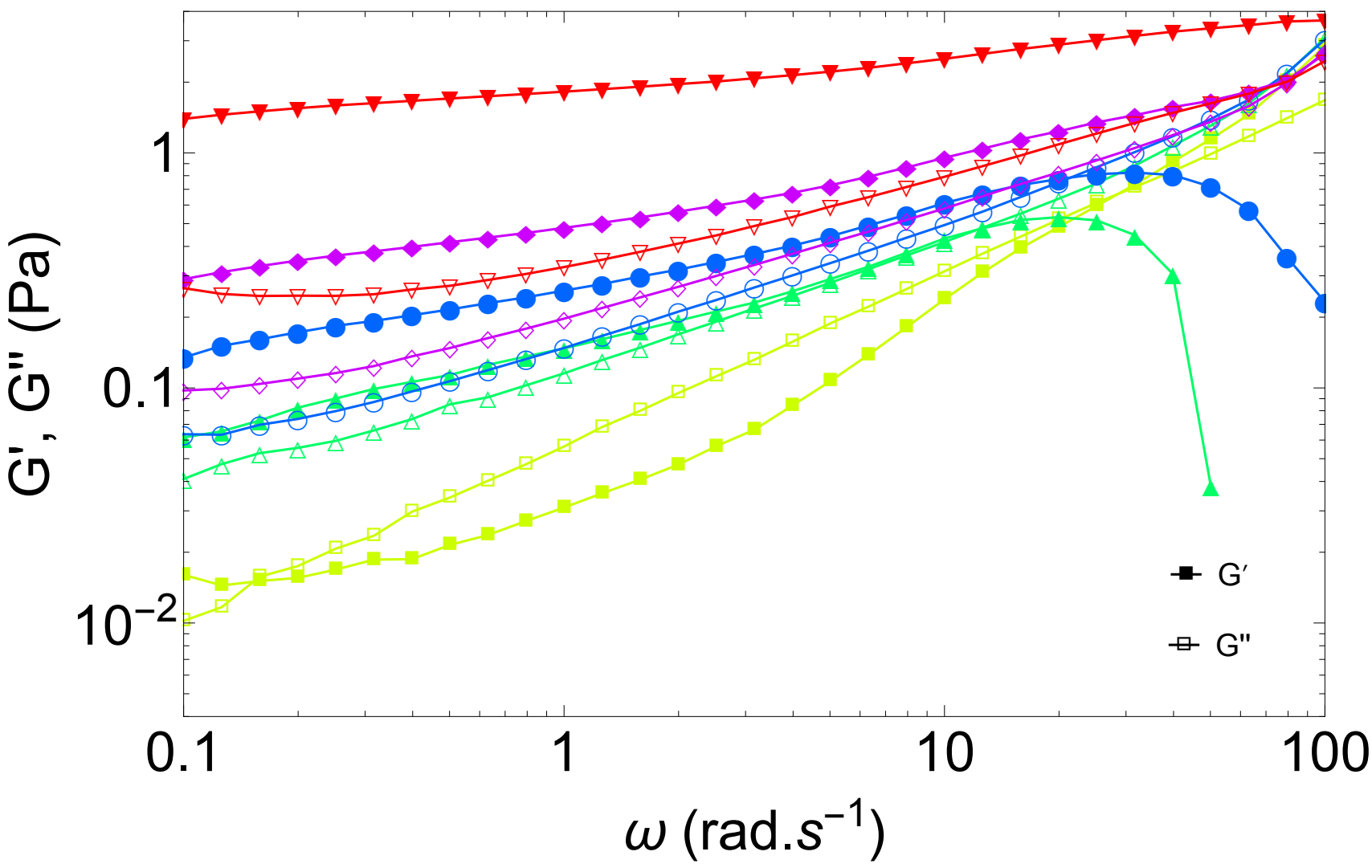
1
0.1
10^{-2}
0.1
1
10
100
G', G" (Pa)
ω (rad.s^{-1})
G′
G"

c)

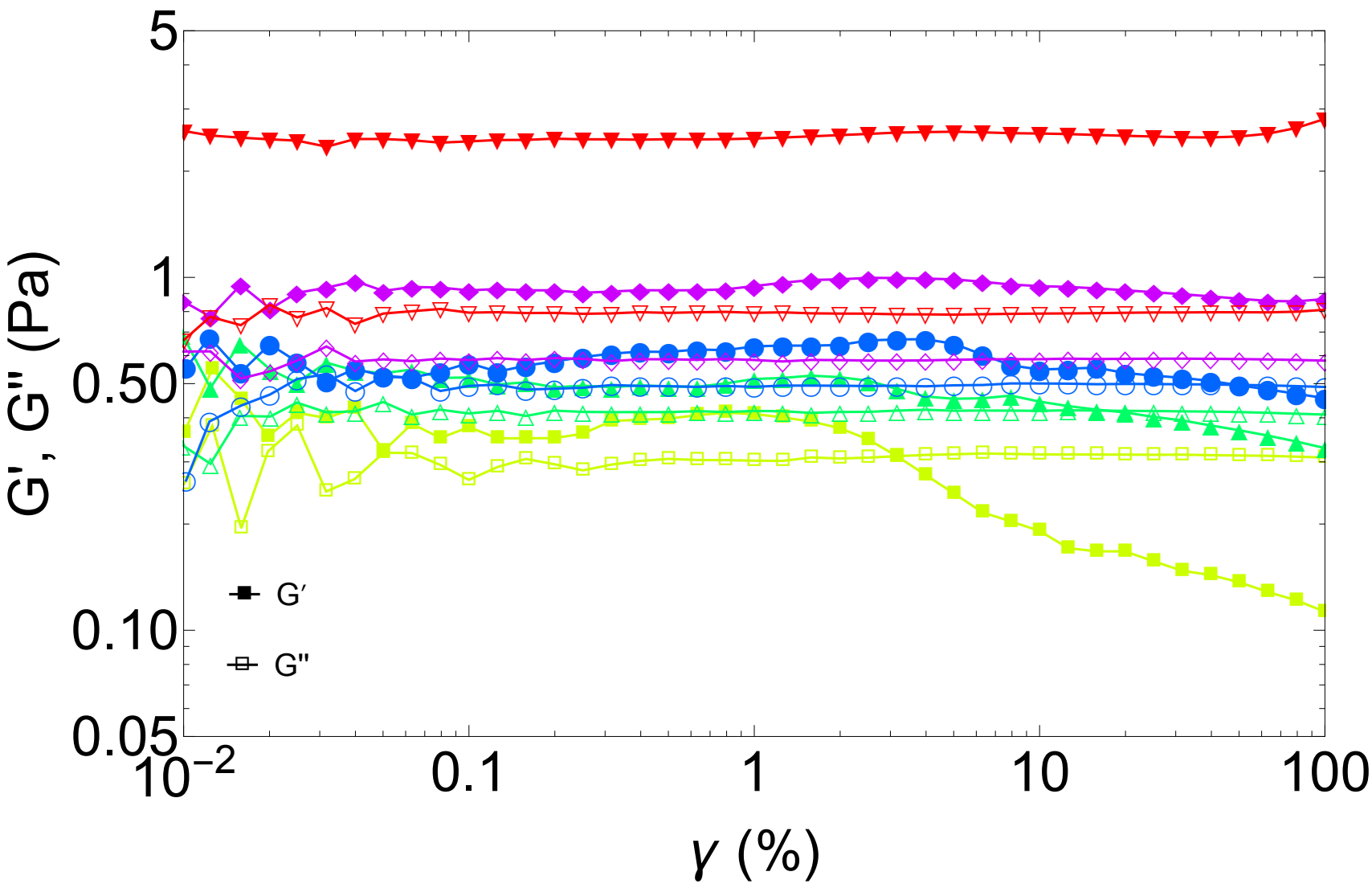
5
1
0.50
0.10
0.05
10^{-2}
0.1
1
10
100
G', G" (Pa)
γ (%)
G′
G"

Accepted to J. Chem. Phys. 10.1063/5.0129276

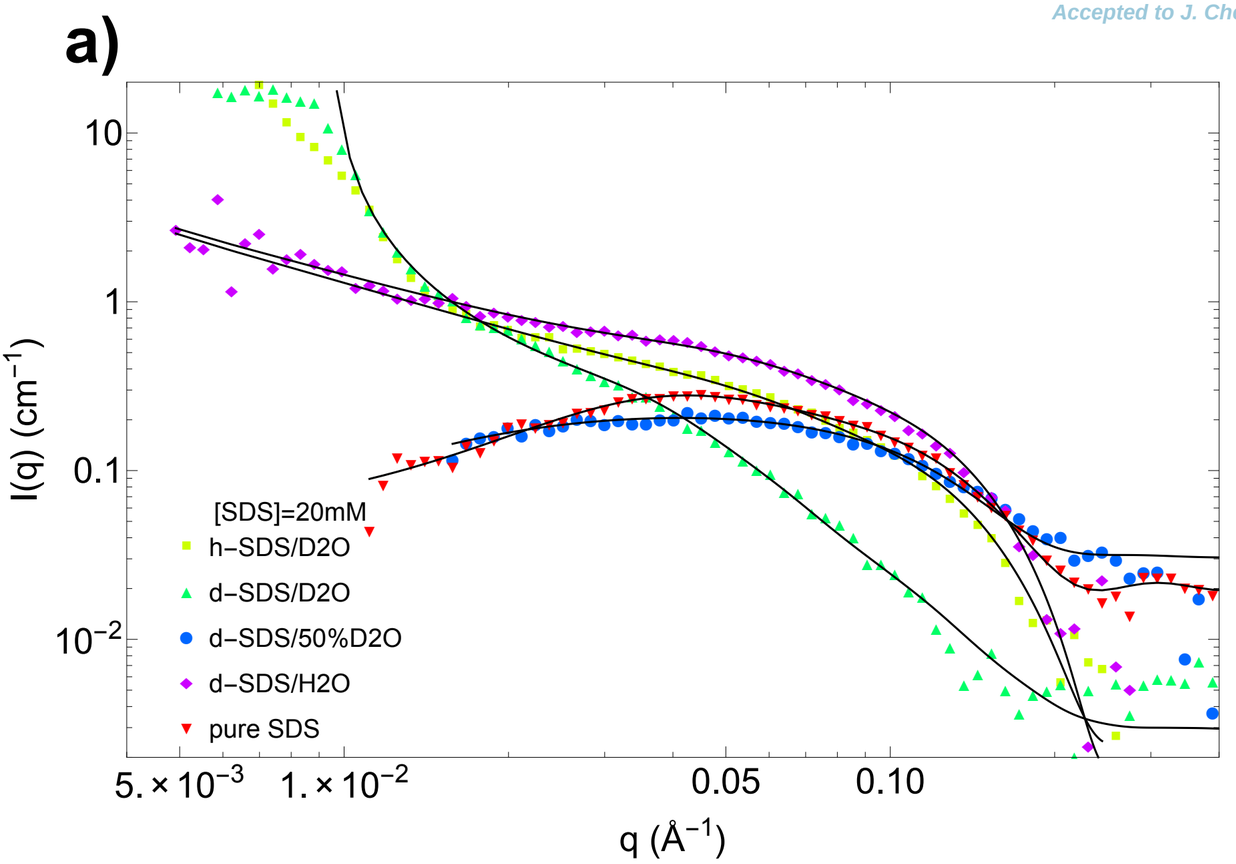

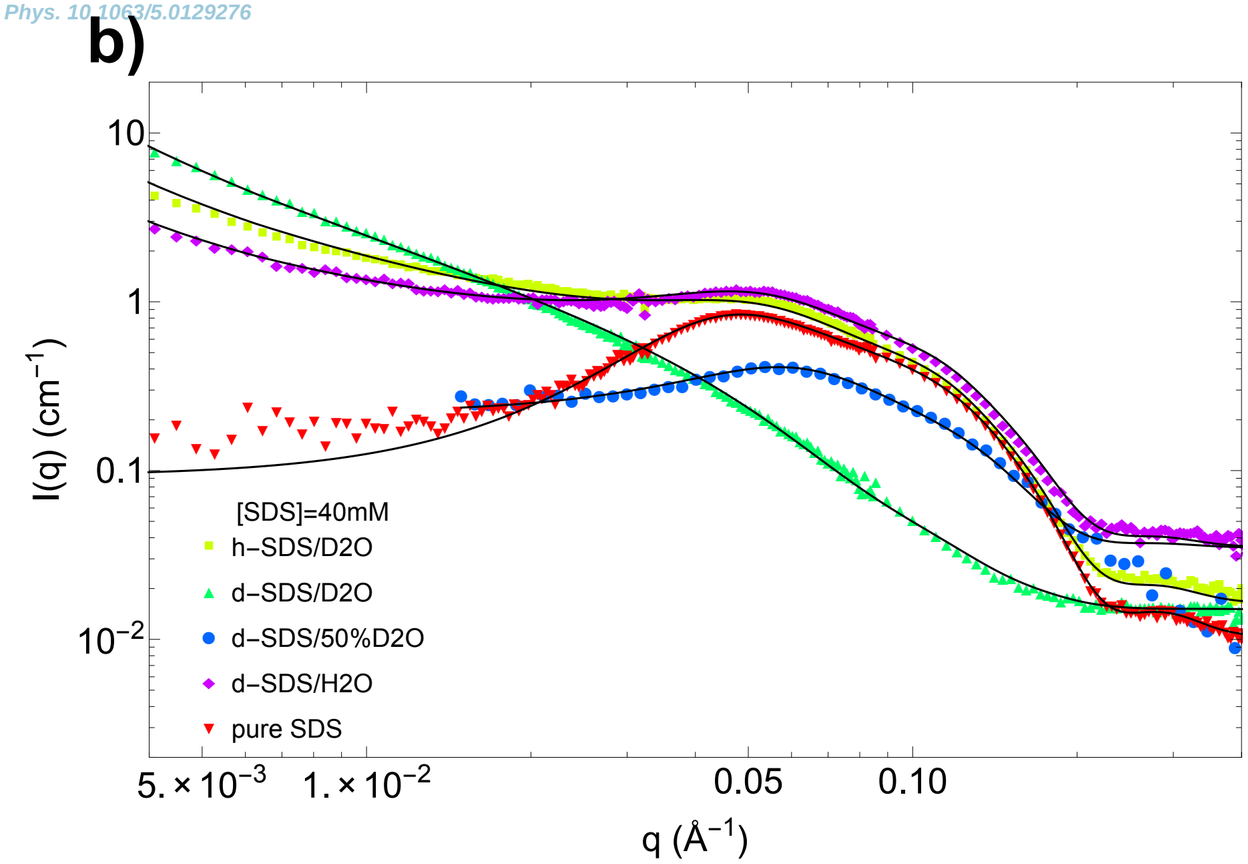

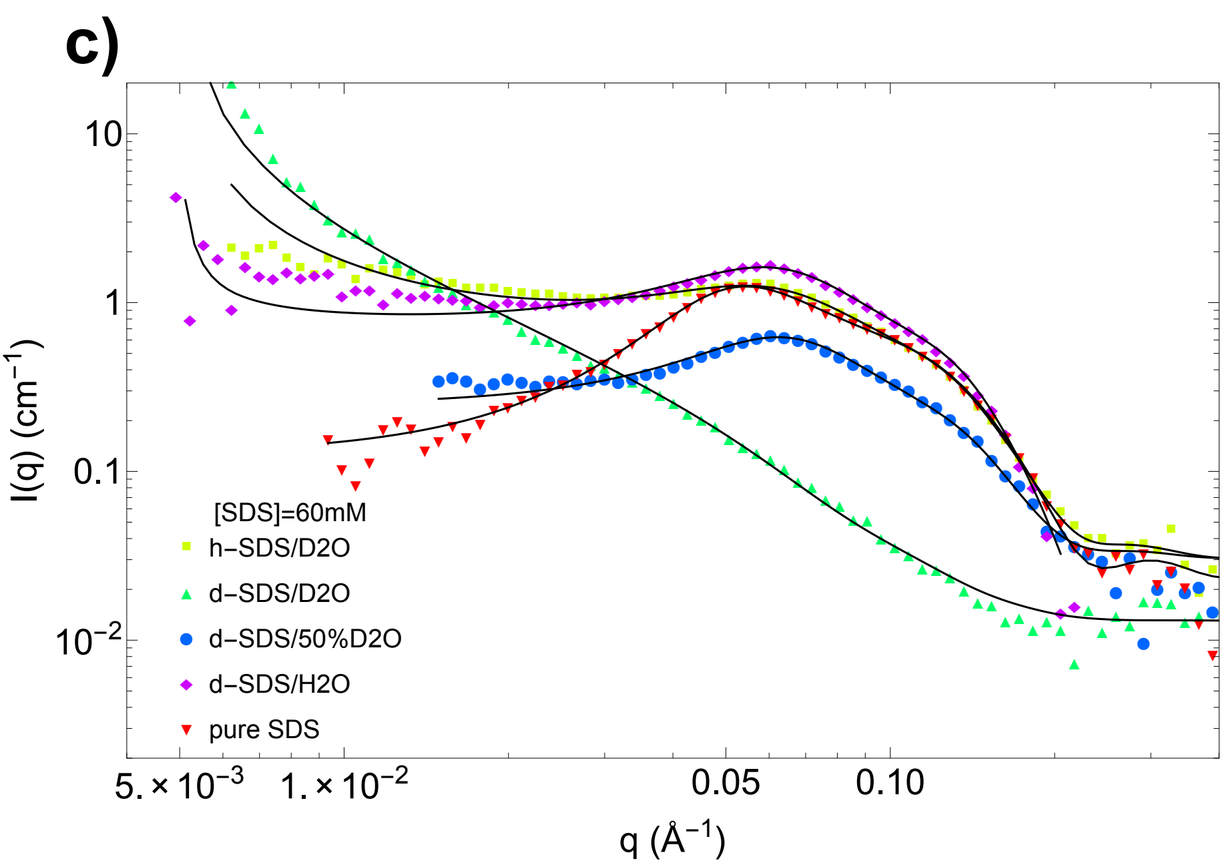

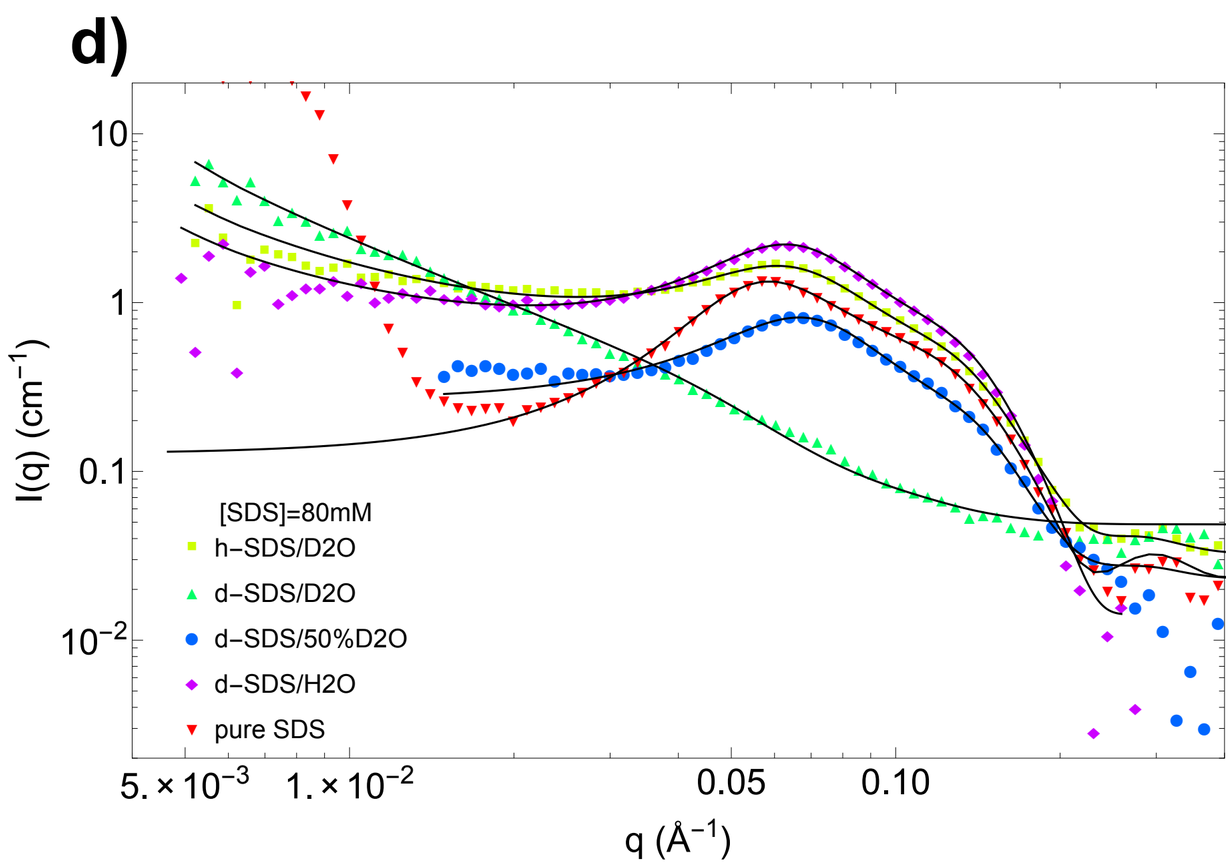

a)

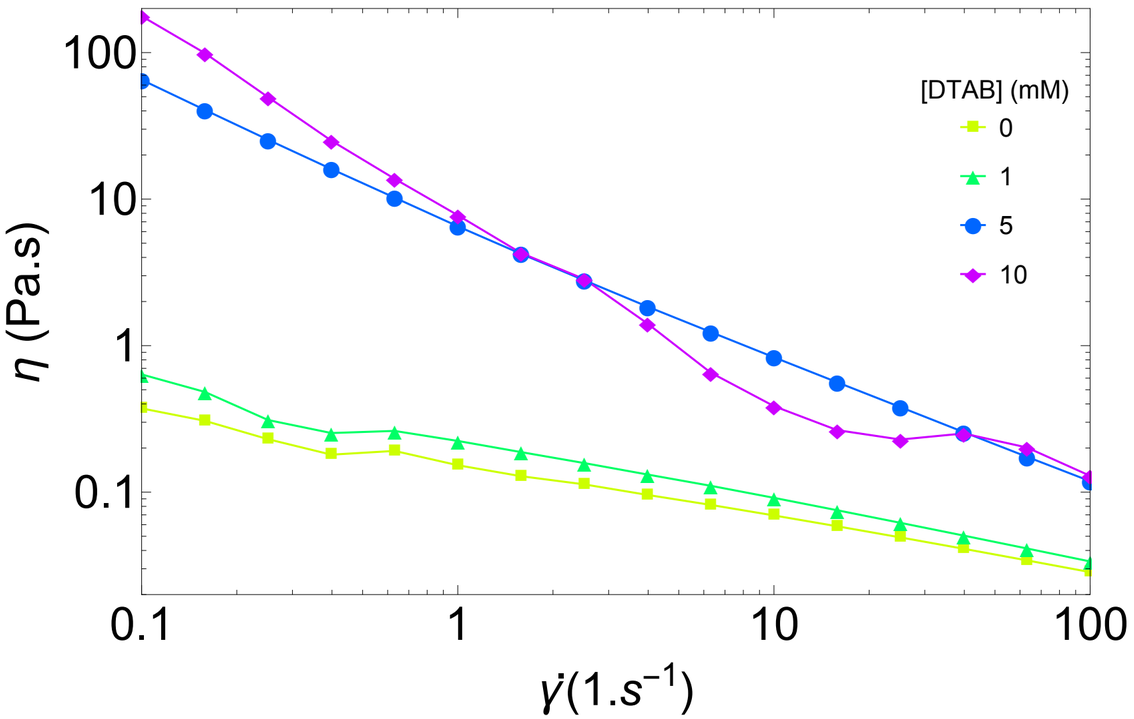
100
10
1
0.1
η (Pa.s)
0.1
1
10
100
γ̇(1.s⁻¹)
[DTAB] (mM)
0
1
5
10

b)

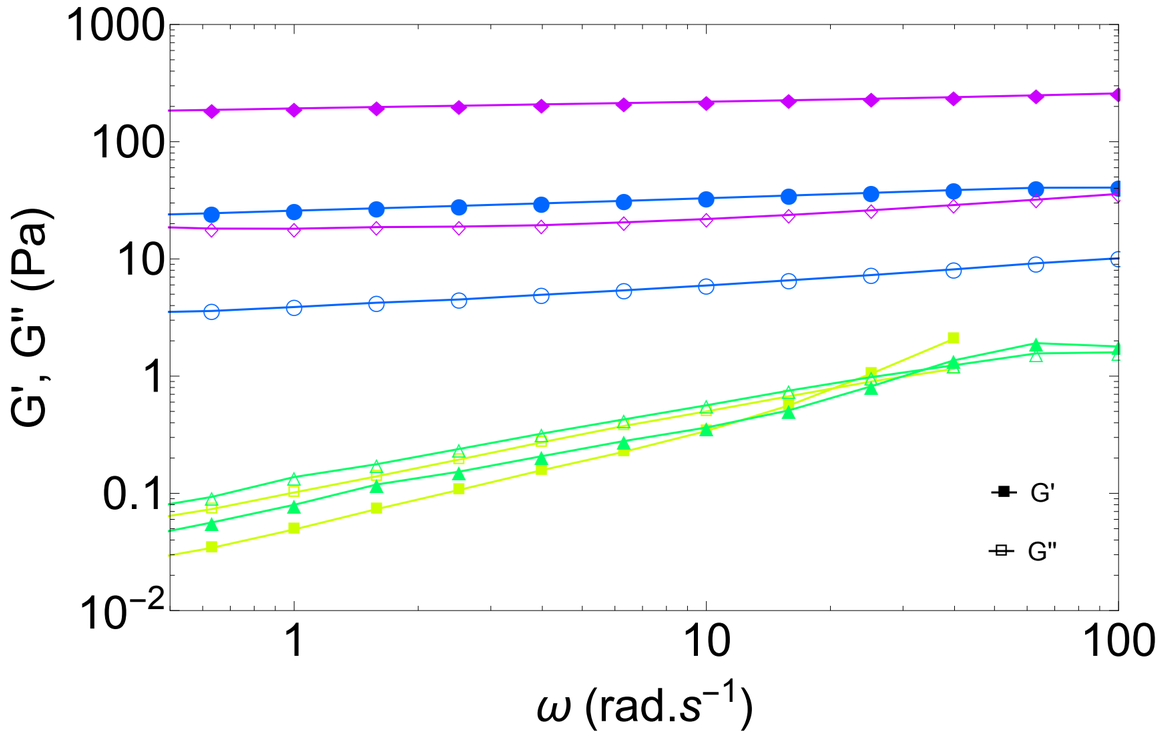
1000
100
10
1
0.1
10⁻²
G', G'' (Pa)
1
10
100
ω (rad.s⁻¹)
G'
G''

c)

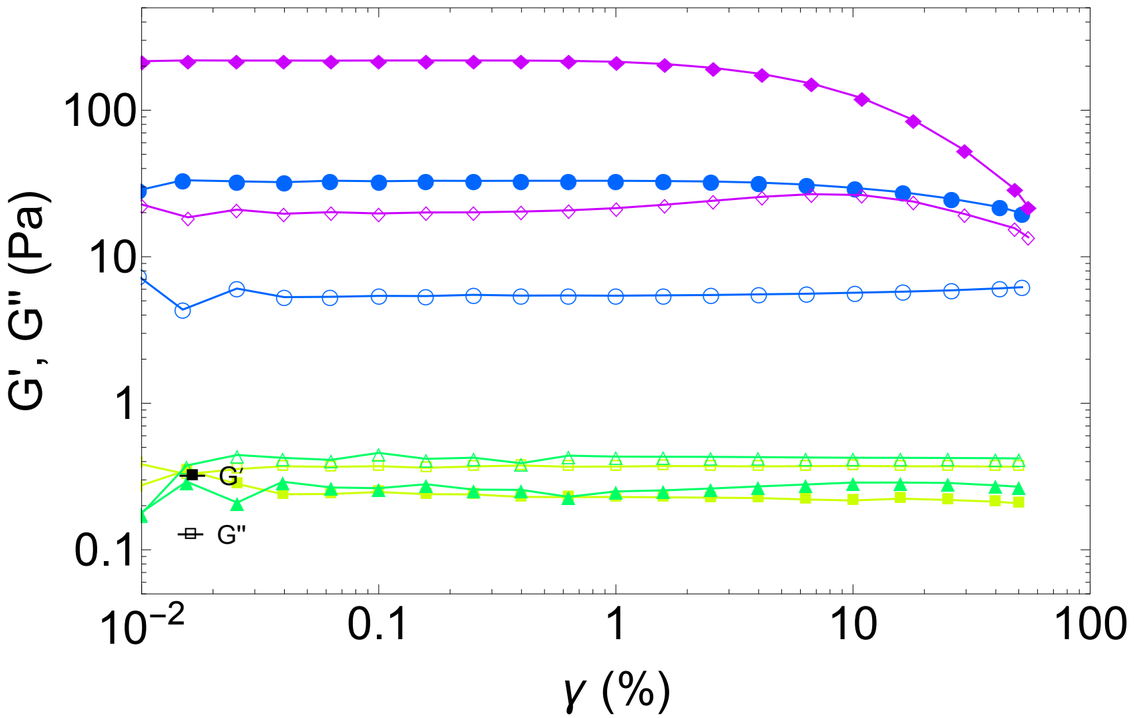
100
10
1
0.1
G', G'' (Pa)
10⁻²
0.1
1
10
100
γ (%)
G'
G''

d)

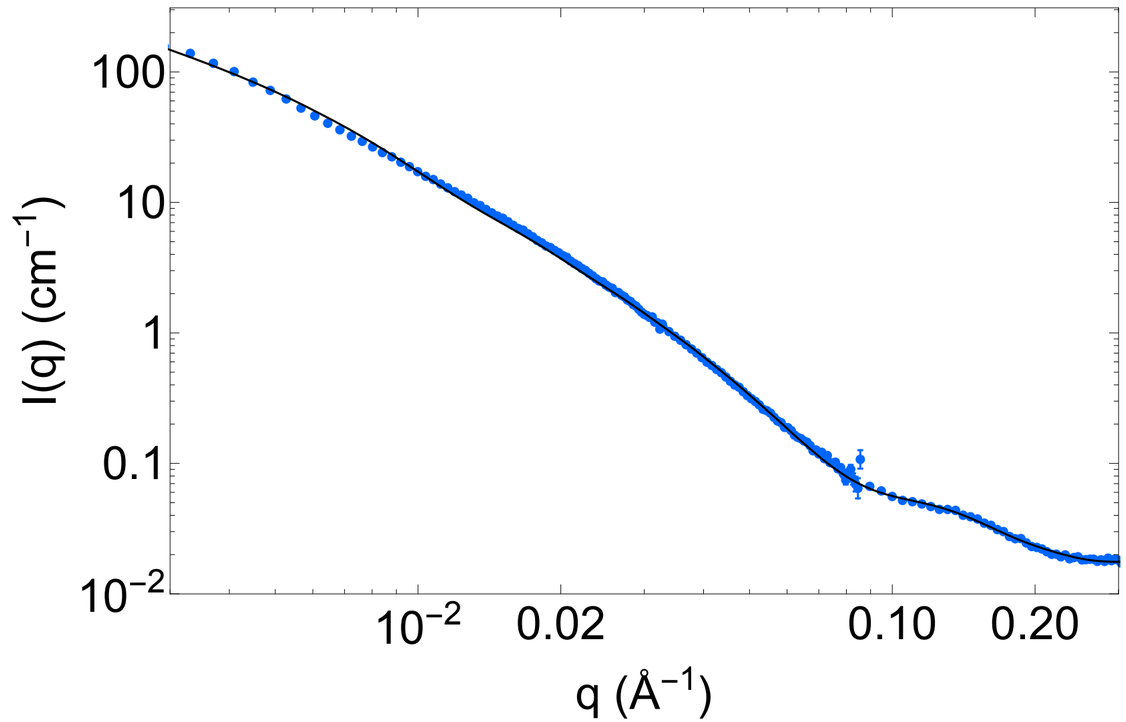
100
10
1
0.1
10⁻²
I(q) (cm⁻¹)
10⁻²
0.02
0.10
0.20
q (Å⁻¹)

a)

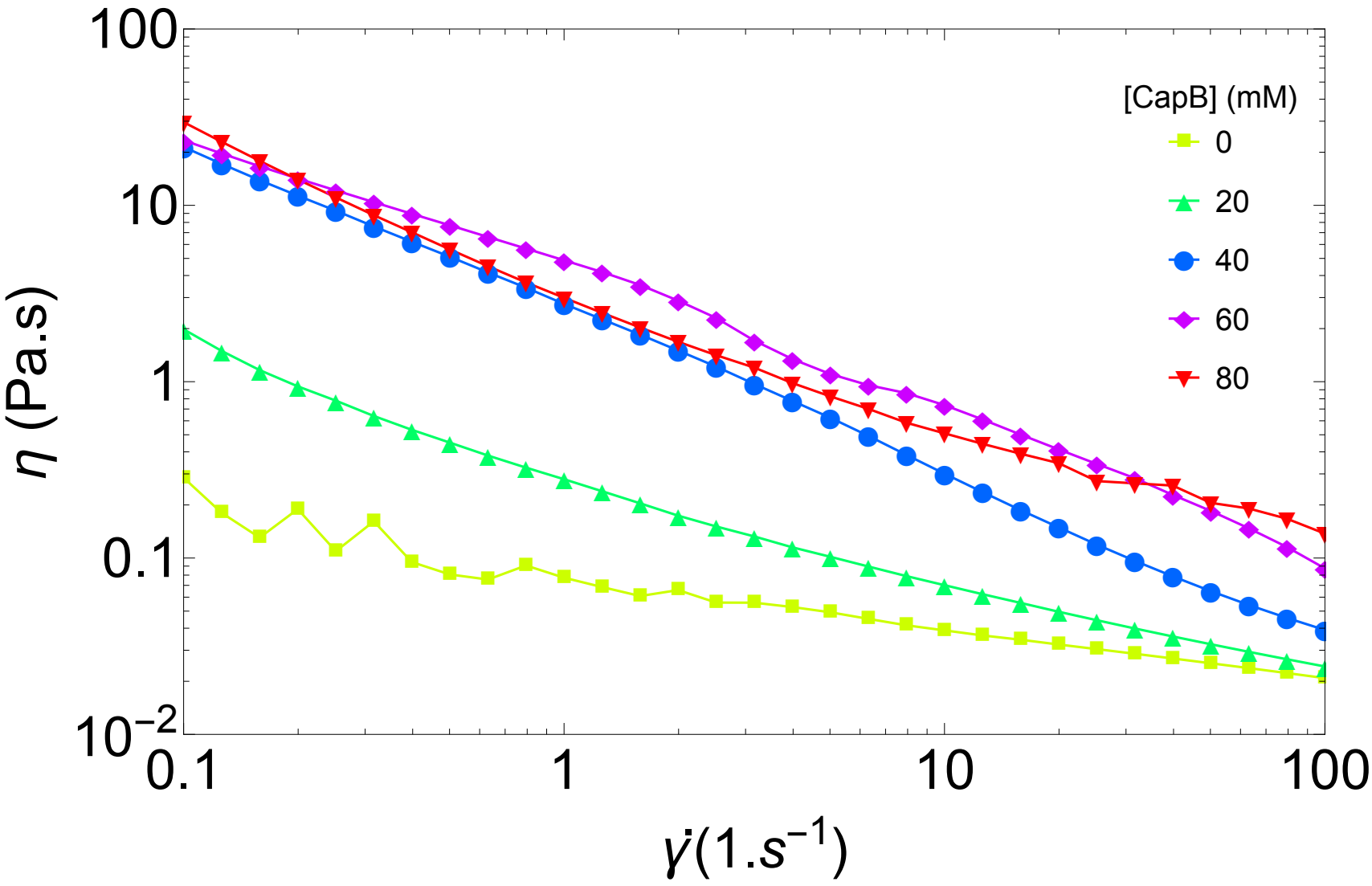
100
10
1
0.1
10^{-2}
0.1
1
10
100
η (Pa.s)
$\dot{\gamma}(1.s^{-1})$
[CapB] (mM)
0
20
40
60
80

b)

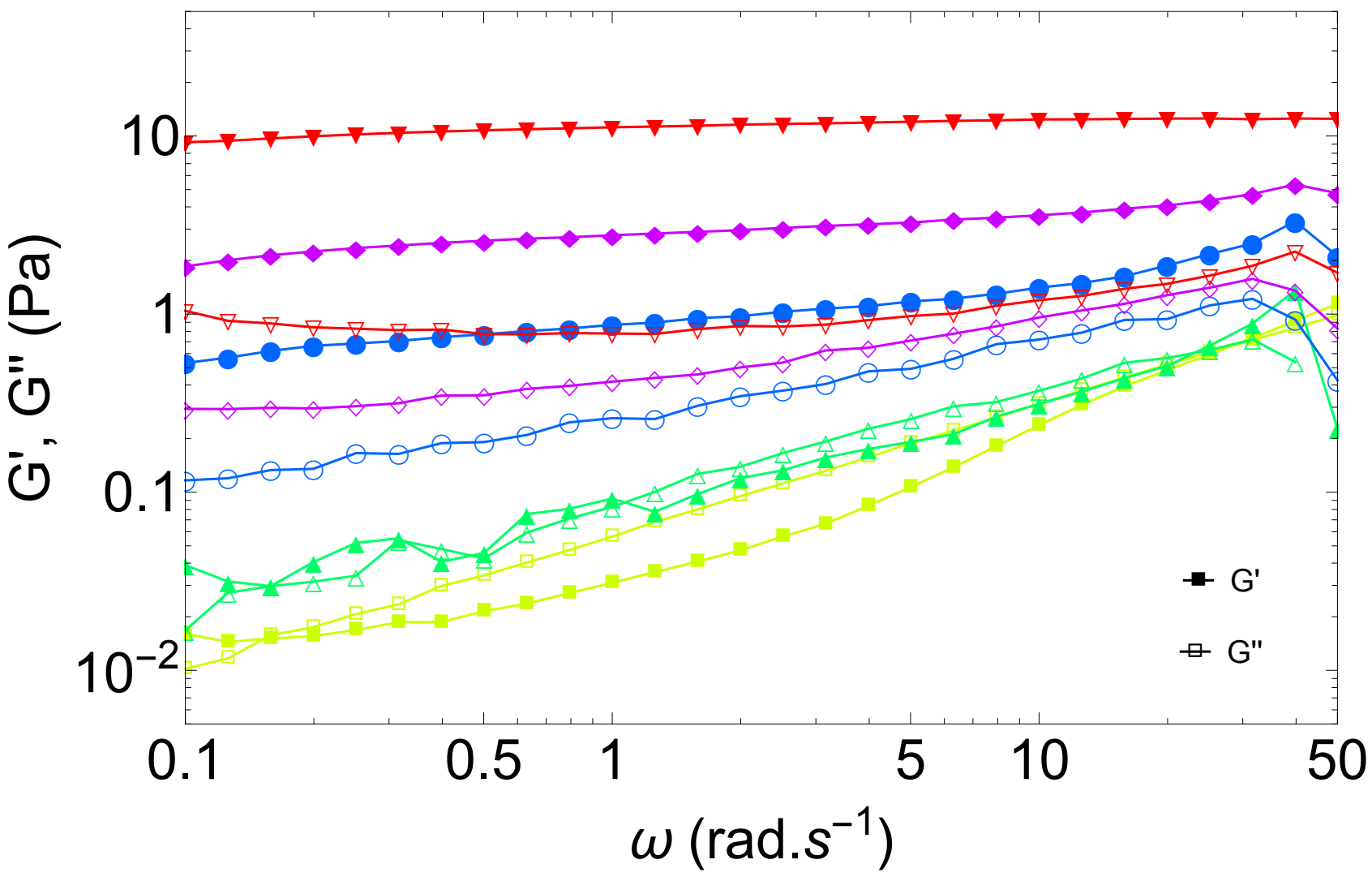
10
1
0.1
10^{-2}
0.1
0.5
1
5
10
50
G', G" (Pa)
ω (rad.s^{-1})
G'
G"

c)

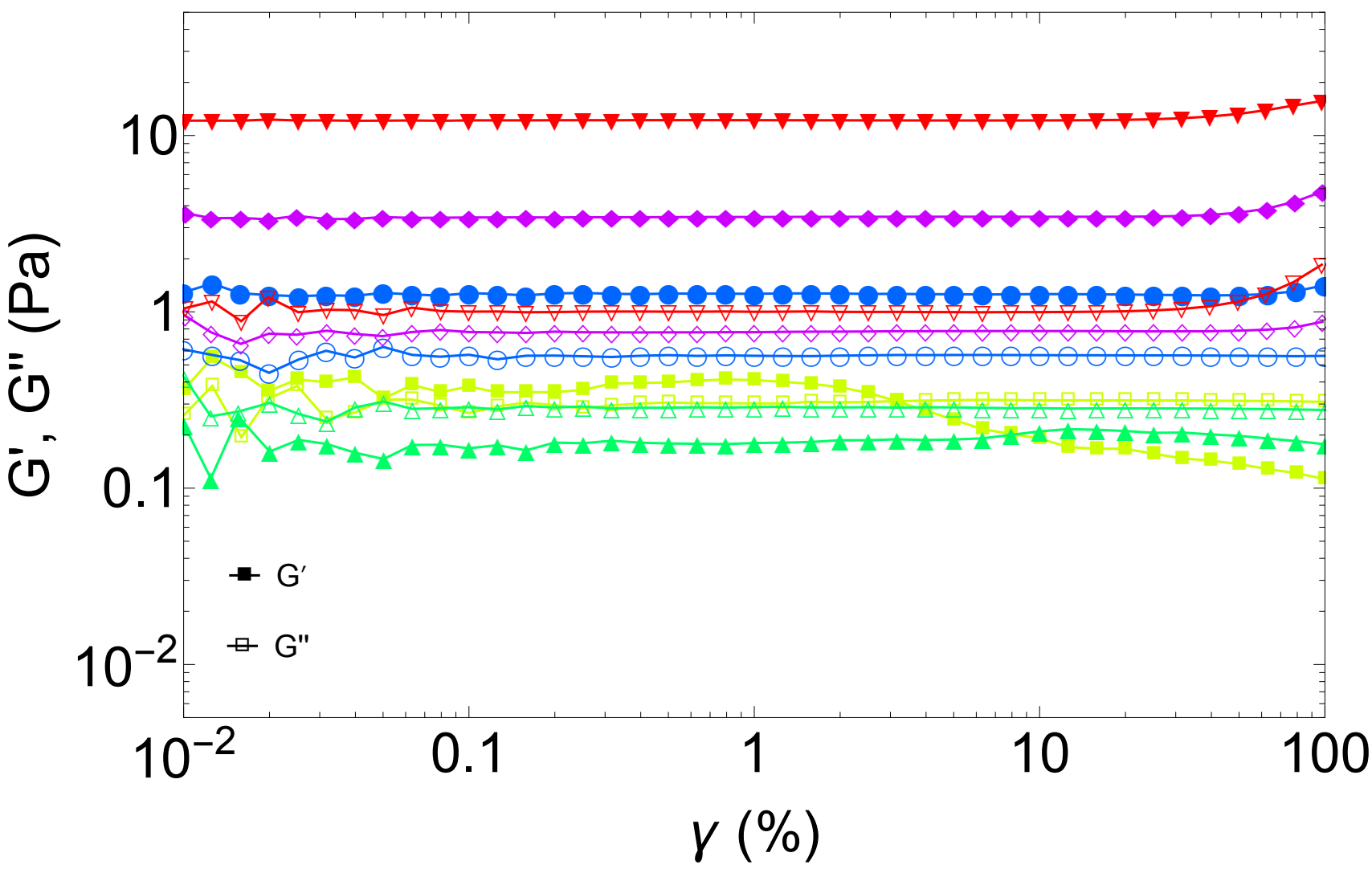
10
1
0.1
10^{-2}
10^{-2}
0.1
1
10
100
G', G" (Pa)
γ (%)
G′
G"

Accepted to J. Chem. Phys. 10.1063/5.0129276